学位論文（博士）

Enhanced drug skin permeability by chemical enhancers and ionic liquid

2023.9

星薬科大学大学院 薬学研究科

総合薬科学専攻

薬品物理化学

Xu Qihui

List of Contents

List of Publications

1. Qihui Xu, Yifan Wu, Hiroki Saito, Yuki Ofuchi, Haruna Setoyama, Takayuki Furuishi, Kaori Fukuzawa, Etsuo Yonemochi, Promoting activity of terpenes on skin permeation of famotidine, *Chem. Pharm. Bull.*, 71 (2), 111-119 (2023).

The content of this manuscript is used in "I. Promoting activity of terpenes on skin permeation of Famotidine".

2. Qihui Xu, Takayuki Furuishi, Kaori Fukuzawa, Etsuo Yonemochi, Physicochemical Properties and Transdermal Absorption of a Flurbiprofen and Lidocaine Complex in the Non-Crystalline Form, *Pharmaceutics*, 15(2), 318 (2023).

The content of this manuscript is used in "II. Transdermal absorption of a Flurbiprofen and Lidocaine complex in the non-crystalline form".

Abbreviations

ATR-FTIR	Attenuated total reflection Fourier transform infrared spectroscopy
^{13}C DD	^{13}C dipolar decoupling
DESs	Deep eutectic solvents
DSC	Differential scanning calorimetry
FDA	Food and Drug Administration
FLU	Flurbiprofen
FMT	Famotidine
GERD	Gastroesophageal reflux disease
GRAS	Generally Recognized As Safe
H2	Histamine-2
HEC	Hydroxyethyl cellulose
HPC	Hydroxypropyl cellulose
HPLC	High performance liquid chromatography
HPMC	Hydroxypropyl methylcellulose
IDM	Indomethacin
ILs	Ionic liquids
IPA	Isopropyl alcohol
LDC	Lidocaine
MAS	Magic-angle spinning
^{15}N CP	^{15}N cross-polarization
NMR	Nuclear magnetic resonance
NSAID	Nonsteroidal anti-inflammatory drug
PBS	Phosphate buffered saline
PM	Physical mixture
SC	Stratum corneum
TDDS	Transdermal drug delivery system

General Information

Drugs can be delivered to the human body in different ways, the most common ways are oral and injection [1-3]. However, first-pass elimination by the oral route can reduce the effectiveness of the drug. The injection route prevents the degradation of drug molecules associated with oral drug therapy, but when frequent dosing is required, the patient is prone to pain and will reduce patient compliance [4-6]. Compared with the above two methods, the transdermal drug delivery system (TDDS) can not only prevent the degradation of drugs but also achieve a painless effect in the whole process, which is superior to oral administration and subcutaneous injection [7, 8]. TDDS is a drug delivery system that takes the skin as the delivery route, delivers the drugs to local tissue or systemic blood circulation, and plays a local or systemic effect [9, 10].

TDDS is an alternative to minimize the limitations associated with oral and parenteral administration of drugs [11]. At present, TDDS for various drugs such as nicotine patches, estradiol, fentanyl, lidocaine, and rotigotine have been developed and approved by the US Food and Drug Administration (FDA) [12, 13]. However, the skin, which is the largest tissue in the human body, is a barrier against the extent and rate of drug absorption by TDDS. Stratum corneum (SC) is the superficial layer of the epidermis and the primary diffusion barrier of the skin [14]. SC consists of keratinocytes embedded in a lamellar lipid matrix, mainly comprising ceramides (41%), cholesterol (27%), cholesteryl esters (10%), and fatty acids (9%), with a small fraction of cholesterol sulfate (2%) [15, 16]. Intercellular, intracellular, and follicular pathways are the three main permeation routes through the SC [17].

To overcome these problems, over the past few decades, many approaches have been developed to enhance transdermal delivery. From the first-generation of TDDS using traditional patches to the second-generation of TDDS and then to the third generation of TDDS, high technology is used to promote the penetration of drugs into the skin, including transdermal penetration enhancers [18]. Following oral administration and injection, TDDS has become the third-largest route of drug delivery, forming a new trend of drug administration. Particularly, TDDS can increase the skin permeation of drugs in the following ways: (1) Changing the structure and fluidity of the SC; (2) Enhancing the dissolution characteristics of

the skin to be delivered (increase the distribution coefficient of the drug in the skin and the diffusion of the drug in the SC); (3) Disorganization of SC lipid alkyl chain; (4) Local separation of lipid domains to create hydrophilic pores in the SC itself and establish a drug reservoir.

In recent years, TDDS has developed rapidly, and researchers have developed a variety of physicochemical methods to facilitate the transdermal delivery of drugs. The main ones are (1) Chemical enhancers. Many effective chemical enhancers disrupt the highly ordered bilayer structures of the intracellular lipids found in SC by inserting amphiphilic molecules into these bilayers to disorganize molecular packing or by extracting lipids using solvents and surfactants to create lipid-packing defects of nanometer dimensions [19]. (2) Electroporation. The electric field applied during electroporation provides the electrophoretic drive in a few milliseconds and this diffusion through the long-lasting electroporation can last for several hours, such that transdermal transport can be increased by orders of magnitude for small molecule drugs, peptides, vaccines, and DNA [20]. (3) Ultrasound. Ultrasound-generated bubbles oscillate and collapse at the skin surface, which generates localized shock waves and liquid microjets directed at the SC [21]. This disrupts SC lipid structure and thereby increases skin permeability for up to many hours without damaging deeper tissues. (4) Microneedles. It can increase skin permeability by creating micron-scale pathways into the skin and can actively drive drugs into the skin either as coated or encapsulated cargo introduced during microneedle insertion or via convective flow through hollow microneedles [22]. (5) Ionic liquids (ILs). ILs can enhance transdermal transcellular and decellular transport, bypass the barrier of the SC, and destroy cell integrity. Hydrophilic ILs act by opening tight junctions in the SC, mainly by enhancing fluidization in protein and lipid regions to promote paracellular transport. Hydrophobic ILs improve their distribution into the epithelial membrane by providing channels, thereby promoting the transcellular transport of lipid regions [23].

Transdermal chemical enhancers are most commonly used to help drugs penetrate the skin. Due to their high enhancement effect and low skin irritation, terpenes of natural origin are now receiving much attention in pharmaceutical and cosmetic formulations as penetration enhancers [24, 25]. Terpenes, primarily extracted from medicinal plants, are volatile compounds with molecular components that are composed of only carbon, hydrogen and oxygen atoms.

The basic chemical structure of terpenes consists of a number of repeated isoprene (C_5H_8) units which are used to classify terpenes. They act on the polar hydrophilic end of the lipid bilayer in SC, destroy the hydrogen bonding network, increase lipid fluidity, and extract lipids to form new polar channels [26]. They are generally regarded to be safer compared to synthetic chemical enhancers which include surfactants, fatty acids/esters, and solvents [25]. Furthermore, a few terpenes (e.g., 1,8-cineole, menthol, and menthone) are included in the list of Generally Recognized As Safe (GRAS) agents issued by the US FDA [27].

ILs and deep eutectic solvents (DESs) have emerged as medications with potential use as facilitators of dermal absorption [23, 28]. ILs and DESs can increase skin permeability by increasing the partition coefficient of the administered drug or its thermodynamic action and momentarily modifying the composition of the SC by breaking down the lipid structure [29-31]. Other enhancement mechanisms, such as decreased melting point and increased membrane solubility, are believed to be related to the permeation-enhancing capability of coformers such as menthol [32, 33]. Indeed, the oily liquid phase (active pharmaceutical ingredient DES) containing a high drug concentration acts as a reservoir and thus may provide a higher driving force for the diffusion of drug molecules into the skin [34].

In this study, I mainly focused on the use of chemical enhancers and the changing in nature of drugs by making them into ILs to promote the efficiency of transdermal permeation of large molecule insoluble drugs.

I. Promoting activity of terpenes on skin permeation of Famotidine

1. Introduction

Gastroesophageal reflux disease (GERD) is a digestive condition characterized by partially digested foods, acidic stomach juices, and fluid coming up into the esophagus from the stomach. It may affect individuals of any age, including infants. Heartburn occurs when you get a burning sensation in your chest due to stomach acid going up into the throat. It develops into GERD if it goes on for some time [35]. Some of the most common symptoms were trouble swallowing or painful swallowing, a feeling of food stuck in the throat, abdominal or chest pain, and blood in the vomit or black and tarry stools [36].

Histamine-2 (H2) receptor blockers are also frequently used to relieve the symptoms of GERD [37]. The frequent exposure to stomach acid can irritate the esophagus and lead to uncomfortable symptoms as described.

Famotidine (FMT) is a competitive H2 receptor antagonist that inhibits gastric acid secretion for the treatment of GERD. It is used via orally route associated with gastric acid secretion for GERD patients [38]. But, FMT is usually administrated as orally, considering symptoms of GERD as mentioned previously, it seems to be better for the GERD patients to take FMT thorough parenteral administration. Moreover, following oral administration, the absorption of FMT was dose-dependent and insufficient. The oral bioavailability ranges from 40–50%, and the C_{max} is reached in 1–4 h post administration. The elimination half-life is approximately 2–4 h, which is expected to increase nonlinearly in patients with decreased renal function [39]. Due to the adverse effects of the central nervous system, longer dosing intervals or reduced doses may be used instead to adjust for the resulting longer elimination half-life of FMT [40, 41]. Intravenous formulations have local adverse effects such as irritation at the injection site; moreover, frequent administration results in low patient compliance. Thus, development of potential dosage form of FMT is required to promote drug absorption as well as improve GERD patient compliance.

TDDS is an alternative to minimize the limitations associated with oral and parenteral administration of drugs [11]. At present, TDDS for various drugs such as nicotine patches,

estradiol, fentanyl, lidocaine, and rotigotine have been developed and approved by the US FDA [12, 13]. Intercellular, intracellular, and follicular pathways are the three main permeation routes through the SC [42]. FMT has a small partition coefficient (logP) value, indicating that it is a hydrophilic drug, which prefers to pass through the SC using the intracellular pathway through the corneocytes [43]. However, according to its chemical structure and experimental data, water solubility of FMT is very low [44]. These findings suggest difficult penetration of FMT through SC, thus indicating the assistance of other means to penetrate. To date, there have been few reports of transdermal studies of FMT. K. Mehra et al [45]. had developed transferosomes as a transdermal delivery system for delivery of FMT and had optimal permeation flux of 22.4 μg/cm^2/hour. But transferosomes are expensive due to its lipid excipients and equipment needed, as well as its complex processes. It is therefore urgent to find more convenient and inexpensive ways to promote the transdermal efficiency of FMT.

Transdermal absorption enhancers are most commonly used to help drugs penetrate the skin. In this study, I evaluated the effect of three terpenes in promoting the skin penetration of FMT. At present, many studies have confirmed the efficacy and safety of *l*-menthol as a transdermal permeation enhancer. And in some report, novel terpenes borneol and geraniol has shown excellent transdermal promoting effect of drugs. Thus, borneol and geraniol were selected as transdermal absorption enhancers in the present study. Borneol is a traditional Chinese medicine obtained from castoreum and is used in the Chinese plaster. Yang *et al.* [14] investigated the safety and promoting effect of borneolum from three sources on transdermal permeation of compounds with different octanol-water partition coefficient values and molecular weights. Here, the mechanism needs to be investigated further. Geraniol is the primary component of rose oil and possesses a good smell. Its effect as a penetration enhancer for transdermal drug delivery has attracted the attention of many researchers. The percutaneous absorption of geraniol from an oil-in-water emulsion was studied by Doan *et al.* [46] However, there is not much research on their mechanism for promoting transdermal, especially for geraniol. Thus, being a monoterpene, in contrast to the cyclic terpenes *l*-menthol and borneol, geraniol has been selected in the present study to examine the penetration effect of terpenes having different structures on SC.

Collectively, in this study, I used novel compound borneol and geraniol as skin permeation enhancers for developing a novel FMT transdermal system, and to compare the results with commonly used terpene *l*-menthol. Furthermore, elucidated the mechanism of these terpenes by differential scanning calorimetry (DSC) and attenuated total reflectance-Fourier transform infrared spectroscopy (ATR-FTIR) measurements.

2. Materials and methods

2.1. Materials

FMT, hydroxypropyl cellulose (HPC), hydroxyethyl cellulose (HEC), isopropyl alcohol (IPA), *l*-menthol, borneol, and geraniol were purchased from Fujifilm Wako Pure Chemical Co. (Tokyo, Japan). All other chemicals used in this study were of reagent grade.

2.2. Preparation of SC sheet

SC was separated from the excised skin of the abdominal region of hairless mouse (Labskin® Hos: HR-1, 7-weeks-old male, Sankyo Labo Service Co., Tokyo, Japan) by digestion with 0.1% (w/w) trypsin in PBS (pH 7.4) at 37 °C for 24 h. The separated SC was rinsed with purified water and dried *in vacuo*. The SC was incubated in different chemical enhancer-IPA solutions for 1 h at 32 °C and dried at room temperature of about 25 ℃ until it reached an acceptable predetermined weight (125% of the pretreatment weight). Table 1 shows various formulations of the terpene-IPA solutions. Procedures involving animals and their care complied with the regulations of the Committee on Ethics in the Care and Use of Laboratory Animals of Hoshi University.

Table 1 Formulations of terpenes-IPA solution (%)

	IPA	*l*-Menthol	Borneol	Geraniol	Water
Control	30	-	-	-	70
l-Menthol	30	3	-	-	67
Borneol	30	-	3	-	67
Geraniol	30	-	-	3	67

2.3. Skin permeation study

2.3.1. Preparation of hydrogel

HPC and HEC (1%, w/w) and FMT (3%, w/w) were dispersed in purified water and allowed to swell overnight to obtain the hydrogel formulation base. Different terpenes (3%, w/w) dissolved in 30% IPA were added dropwise to the hydrogel formulation base while stirring overnight to obtain a homogeneous FMT hydrogel. Table 2 shows different formulations of FMT hydrogel.

Table 2 Formulations of FMT hydrogel (%)

	FMT	IPA	HPC	HEC	Chemical enhancers			Water
					l-Menthol	Borneol	Geraniol	
Control	3	30	1	1	-	-	-	65
l-Menthol	3	30	1	1	3	-	-	62
Borneol	3	30	1	1	-	3	-	62
Geraniol	3	30	1	1	-	-	3	62

2.3.2. In vitro skin permeation study

Hairless mouse skin (Labskin® Hos: HR-1, 7-weeks-old male, Sankyo Labo Service Co., Tokyo, Japan) was mounted on a Franz-type diffusion cell. The donor cell was fixed facing towards the SC side, while the receiver cell faced towards the dermis side. Phosphate-buffered saline (PBS; pH 7.4; 16 mL) containing 1% acetic acid was heated in a water bath to 32 °C and added to the receiver cell. The prepared hydrogel (1 mL) was applied to the donor cell, and the top of the cell was covered with parafilm. Aliquots containing 8 mL of the receiver solution were collected at predetermined time intervals (every 2 h for 24 h) and replaced immediately; FMT concentration in the samples was measured by high performance liquid chromatography (HPLC).

2.4. DSC measurements

Thermal analysis of SC was performed using DSC (Shimadzu Co., Tokyo, Japan). Five milligrams of SC was placed on aluminum seal pans, and analysis was performed from 20 ℃

to 140 ℃ at a heating rate of 10 ℃/min. All experiments were performed in triplicates. Thermograms were analyzed using the ORIGIN® 2016 software (LightStone Co., Tokyo, Japan).

2.5. ATR-FTIR measurements

ATR-FTIR measurements were carried out using FTIR-4200 spectrometer fitted with ATR PRO (JASCO International Co., Tokyo, Japan). SC sheets were placed on a sample stage containing ZnSe crystal. The contact area with the sample was 1.5 mm^2. The incident angle of the IR radiation was 45°, and the radiation penetrated the sample to a depth of 1–2 μm. All spectra were obtained as an average of 256 scans recorded from 4000 to 600 cm^{-1} at a resolution of 2 cm^{-1}. The sample stage temperature was increased at a heating rate of 1.0 ℃/min to the target temperature ± 0.3 ℃. Spectra were acquired from 20 to 100 ℃ at 5 ℃ increments. All experiments were performed in triplicates. Spectral analysis was performed using the ORIGIN® 2016 software (LightStone Co., Tokyo, Japan). All parameters were determined by fitting a Gaussian function to the IR data.

2.6. HPLC analysis

FMT concentration in the samples was determined using HPLC (Shimadzu Co., Tokyo, Japan) equipped with an auto sampler, an ultraviolet detector, and a C18 column (YMC-Pack ODS-A; 150 × 4.6 mm^2 I.D.). Methanol: 1% acetic acid (30:70, v/v) was used as the mobile phase at a flow rate of 1 mL/min. The injection volume was 20 μL, and scanning was performed at 267 nm at room temperature of about 25 ℃. A calibration curve (peak versus drug concentration) was constructed by running standard FMT solutions in methanol for every series of chromatography samples. Calibration curves were observed to be linear in the range of 25–100 μg/mL.

2.7. Data analysis and statistical evaluation

The cumulative amount of drug permeating through the skin from FMT hydrogel was plotted as a function of time. The cumulative drug permeation (Q_n) was calculated using the following equation (1):

$$Q_n = (C_n \times V_0 + \sum_{i=1}^{n-1} ci \times Vi/S)$$

(1)

where C_n is FMT concentration of the extracted receiver medium, V_0 and V_i represent the volume of the receiver medium and sample, ci is FMT concentration in the sample solution, and S is the effective penetration area (S=2.01 cm^2).

The steady-state flux (J_{ss}) was calculated using the following equation (2) at a steady state:

$$J_{ss} = \frac{\Delta Q_t}{\Delta T \times S}$$

(2)

ΔQ_t is the change in the quantity of the drug (μg) passing through the skin into the receptor compartment. The flux was calculated from the slope of the linear portion of the curve. The lag time was determined by extrapolating the linear portion of the curve to the abscissa, where J_{ss} is the steady-state skin flux in $\mu g/cm^2/h$, S is the active diffusion area in cm^2, Δt is the change in time, and T_{lag} is the lag time in h.

2.8. Statistical analysis

One-way analyses of variance (ANOVA) were used for statistical analysis of the results. Statistical significance was set at $P < 0.05$.

3. Results and discussions

3.1. Skin permeation of FMT

Figure 1 shows the skin permeation results of the two samples with different concentrations of IPA (20% and 30%) and FMT (5% and 3%). The cumulative permeation

curve of FMT showed a similar trend in both 20% and 30% IPA solutions. FMT in 30% IPA solution showed slightly better permeability than that of FMT in 20% IPA solution. The solubility data of FMT in 20% and 30% IPA solutions is shown in Table 3, which indicates almost the same solubility of FMT, with 13.65 μg/mL in 20% IPA solution and 12.12 μg/mL in 30% IPA solution. $AUC_{0\text{-}12h}$ and flux were calculated using the trapezoidal rule from the cumulative permeation versus time curve and are shown in Table 4. Differences in the values of $AUC_{0\text{-}12h}$ among different formulations were insignificant. Moreover, differences in the value of permeability coefficient of the saturated hydrogels based on the flux and solubility were observed to be insignificant.

Table 3 FMT solubility in 20% IPA solution and 30% IPA solution

	Solubility (μg/ml)
IPA 20%	13.65±2.60
IPA 30%	12.12±0.16

Table 4 $AUC_{0\text{-}12h}$ derived from cumulative amount and time curve of IPA 20% and IPA 30%

	$AUC_{0\text{-}12h}$ (μg·h/cm^2)	Flux (μg/cm^2/h)	Permeability Coefficient
IPA 20%	370.13±14.28	6.15±2.62	0.45±0.08
IPA 30%	472.44±26.09	10.86±1.69	0.89±0.11

It was observed that increasing the IPA concentration and simultaneously decreasing the drug concentration resulted in the cumulative amount of FMT versus time curves of almost similar shape. As shown in Table 4, the difference between $AUC_{0\text{-}12h}$ and flux of the two formulations was insignificant. FMT is very slightly soluble in water, slightly soluble in methanol, and freely soluble in glacial acetic acid [46]. The solubility of FMT in IPA solution was relatively low, indicating that both solutions (5% FMT in 20% IPA solution and 3% FMT in 30% IPA) were saturated. This result indicates that IPA had no significant effect on drug solubility. Based on the solubility of FMT in IPA solution (Table 3), it was considered that the thermodynamic activity of FMT in the hydrogel was maximized. Therefore, the two formulations had similar thermodynamic activity and escaping tendency of FMT from the hydrogel, and similar permeation rates (Fig. 1). Moreover, IPA was expected to promote skin permeation of the drug; however, in this study, the skin permeation promoting effect was not observed with increase in the concentration of IPA. Since IPA had only slight effect on drug

solubility and the promotion of drug partition to the skin surface was considered to be the main mechanism for promoting permeation of IPA, different concentrations of IPA had slight effect on partition of FMT to the skin surface. In addition, no other direct action of IPA on the skin surface was observed.

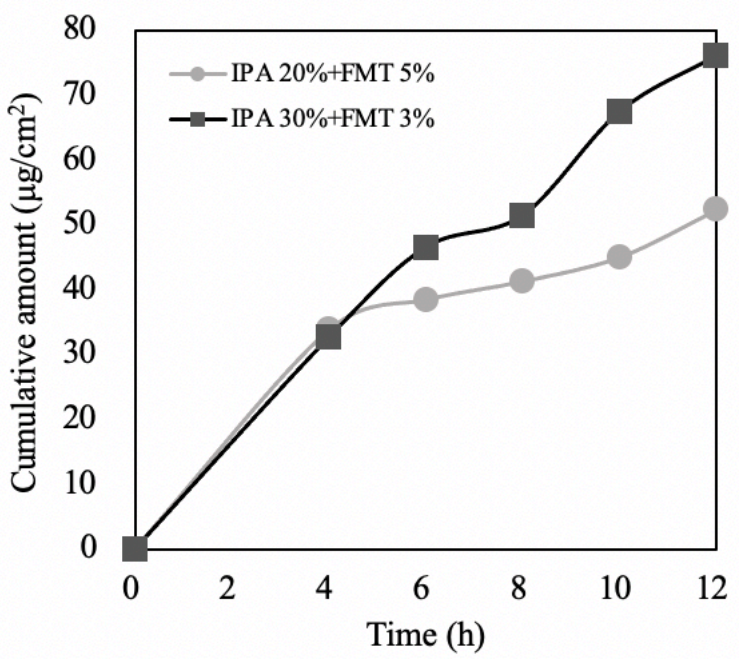

Fig. 1 FMT permeation across the mice skin between different concentration of IPA and FMT. Each point represents the mean ± S.D. (n=3).

3.2. Effects of different terpenes on FMT skin permeation

The results of FMT skin permeation revealed that FMT in IPA solution could not efficiently penetrate the skin. Therefore, other methods are required to promote FMT skin penetration. There are several physical and chemical methods to improve drug permeation, including microneedles, iontophoresis, microemulsions, and penetration enhancers. Among these methods, the use of penetration enhancer is an established and widely used approach. Here, I compared the penetration promoting effect of three terpenes as penetration enhancers.

In order to investigate the effect of terpenes on skin permeation of drugs, *an in vitro* permeation experiment was performed using IPA as a common additive, which was incorporated at 30% into all aqueous hydrogel formulations. The hydrogel formulations, widely used in commercial preparations, were used as dosage forms in this study. The

receiver cell was filled with PBS (pH 7.4) containing 1% acetic acid to ensure sink conditions during the permeation studies.

In the previous experiment, I compared the penetration ability of 5% FMT in 20% IPA and 3% FMT in 30% IPA and found that different concentrations of IPA solution had similar effect on FMT skin permeation. Then, I added terpenes to observe their effects on FMT penetration. Since the three terpenes are hydrophobic compounds, I selected 30% IPA solution as the control group, considering the better enhancement effect of the higher IPA content.

The cumulative amount versus time curve of *in vitro* skin permeation experiments using *l*-menthol, borneol, and geraniol is shown in Fig. 2.

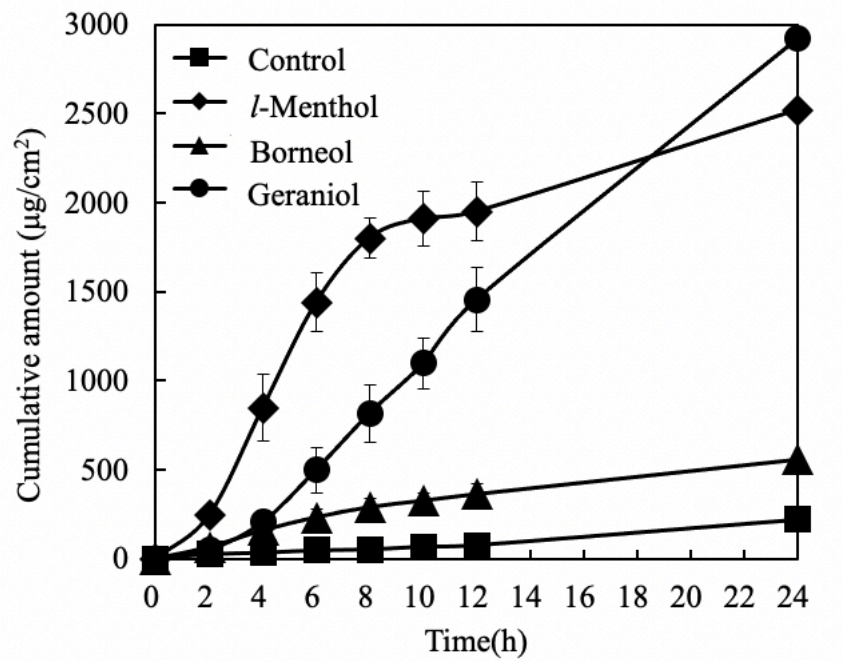

Fig. 2 FMT permeation across the mice skin. Each point represents the mean ± S.D. (n=3). ◆: *l*-Menthol, ▲: Borneol, ●: Geraniol, ■: Control.

These results confirmed that all terpenes had a promoting effect on FMT skin permeation, and the flux of FMT with terpenes was significantly higher than that of the control group in the order of *l*-menthol > geraniol > borneol. The cumulative permeation of FMT reached a steady state after a certain lag time, and it was observed that FMT continuously permeated through the skin. The cumulative permeation of the formulation containing geraniol showed the highest value, which was 13-times higher than that of the formulation containing IPA only

with the lowest permeation. Furthermore, the steady-state flux and lag time, which used to evaluate skin permeability can be calculated according to the Fick's law of diffusion (Equation (2)) from the cumulative permeation versus time curve shown in Fig. 3. Collectively, all terpenes increased FMT transdermal permeation rate compared to the control, and the extent of the increase was proportional to the concentration; however, *l*-menthol showed the highest steady-state flux. In addition, the lag time after using with borneol is shortest, this was followed by *l*-menthol and geraniol. The control group had the longest lag time.

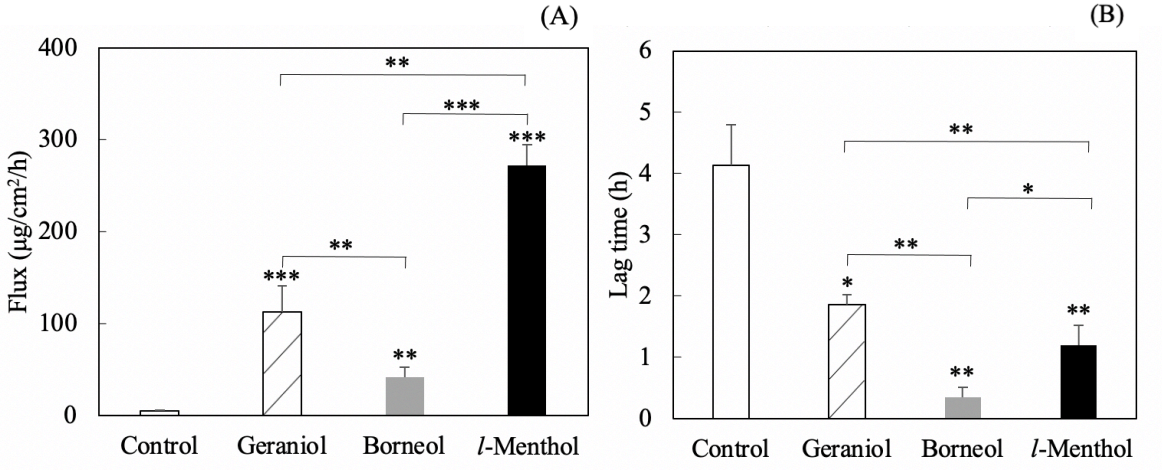

Fig. 3 (A) Steady-state flux and (B) lag time of FMT through hairless mouse skin. Each point represents the mean ± S.D. (n=3). **p*< 0.05, ***p*< 0.01, ****p*< 0.001 vs. Control. Control was SC treated with only IPA 30% formulation.

As shown in Fig. 2, the formulation containing geraniol had the highest cumulative amount. As shown in Fig. 3, the highest flux for *l*-menthol and the relatively shorter lag time also explained this; the higher the flux, the shorter is the lag time. However, comparing with the 24h cumulative curve of FMT, *l*-menthol and geraniol, particularly geraniol, showed a strong effect on FMT permeation. Despite the flux of *l*-menthol, the curve showed that the permeation influence of the FMT with *l*-menthol decreased after around 12h. In contrast, geraniol had a longer effect on FMT transdermal penetration compared to *l*-menthol, resulting in a reverse drug cumulative amount beyond *l*-menthol at 24h. In the case of borneol, the

shortest lag time of FMT was shown, which mean that borneol would be a possible option to promote rapid onset of drug action that leads to faster therapeutic effects, but borneol had only slight effect compared with the control group. This means that sufficient plasma drug concentration would not be reached. Moreover, at the end of the skin permeation study using the borneol, I observed a few white particles of residual drug on the skin surface. This indicated that thermodynamic of FMT was maximum or not change, while borneol didn't affect the solubility of FMT in the gel. Although it was not straightforward to draw conclusions, I assumed that the transdermal enhancement effect of borneol related to the drug solubility in donor compartment on FMT had been maximized, as will be discussed later in the text. This indicated that even though the lag time was short, the transdermal efficiency of FMT was affected by the small flux. The lag times for *l*-menthol and geraniol were also significantly shorter compared to the control group, suggesting that terpenes contributed significantly to the rapid onset of action of FMT. This may be attributed to the differences in their chemical structures and the mechanism underlying their penetration enhancement effects on SC. The logP values of *l*-menthol, geraniol, and borneol were 3.40, 3.56, and 3.24, respectively [14, 46]. They are hydrophobic compounds with nearly same logP values. Therefore, it is speculated that differences in the mechanism underlying their penetration enhancement effects is mainly attributable to this result, which was further elucidated by DSC and FTIR measurements. For clinical use, the predictable permeation rate and time are required for an efficient formulation. The cumulative amount of FMT with *l*-menthol, borneol and control group gradually become stable at around 12h, while the cumulative amount of geraniol still showing an increasing trend. This also contributed to the longer effect of geraniol on FMT transdermal penetration. These properties are beneficial to the patients, making it a favorable compound for FMT transdermal delivery.

3.3. Effects of terpenes on DSC profile of SC

DSC is a thermal analysis method for studying the relationship between sample properties and temperature. When SC was subjected to DSC scanning, several endothermic peaks appeared. The structure and mechanism of action of penetration enhancers on SC can be

elucidated by studying the changes in these peaks. DSC is commonly used to study the lipid phase transition properties of SC [47].

The effects of chemical enhancers on thermotropic behavior of intercellular lipids in SC can be observed by DSC thermograms. The phase transition of SC is known to be liquid crystallization of orthorhombic packing at a temperature of 40 ℃, dissolution of long-period lamella at 50 ℃, melting of short-period lamella, and liquid crystallization of hexagonal packing at 70 ℃ [48]. In contrast to the short periodicity phase, the presence of long periodicity phase is unique for SC lipid organization, which suggests that this phase plays an important role in the cutaneous barrier function [47].

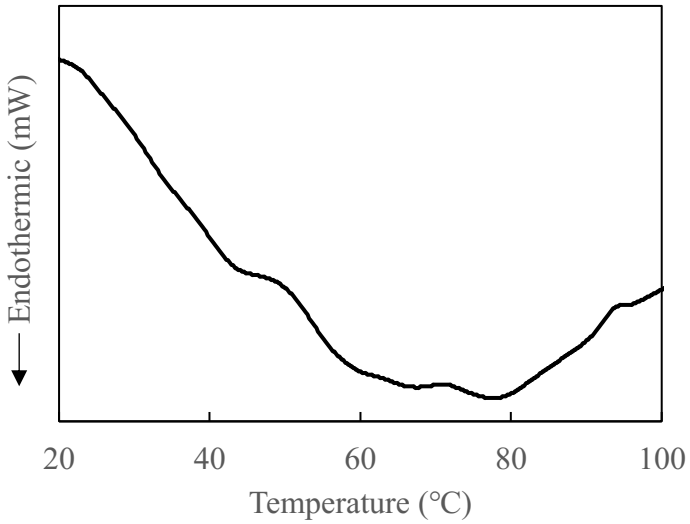

Fig. 4 The endothermic DSC curve of 30% IPA solution.

After applying different terpenes on SC, the peak position of intercellular lipids was observed, and the endothermic curve of 30% IPA solution is shown in Fig. 4. The endothermic peak was observed at approximately 40 ℃, 50 ℃, and 70 ℃. The endothermic curve was then analyzed for second-order differentiation, and the phase transition temperature was determined. The changes in phase transition temperature due to the application of terpenes are shown in Fig. 5. The results indicated that the phase transition temperature of all chemical enhancers applied to SC was lower that of the control group. The phase transition temperature of *l*-menthol and geraniol was observed at 40 °C, 50 °C, and 70 °C, and at 50 °C and 70 °C, respectively. Among the three terpenes, *l*-menthol significantly reduced the three

typical phase transition temperatures in SC. Geraniol and borneol did not show a significantly low phase transition temperature at 40 °C, but the phase transition temperature of geraniol at approximately 50 °C was the largest change among the three chemical enhancers. For borneol, there were only slight changes at 50 °C, and it showed a typical temperature change at approximately 70 °C compared with the control group and the other two enhancers.

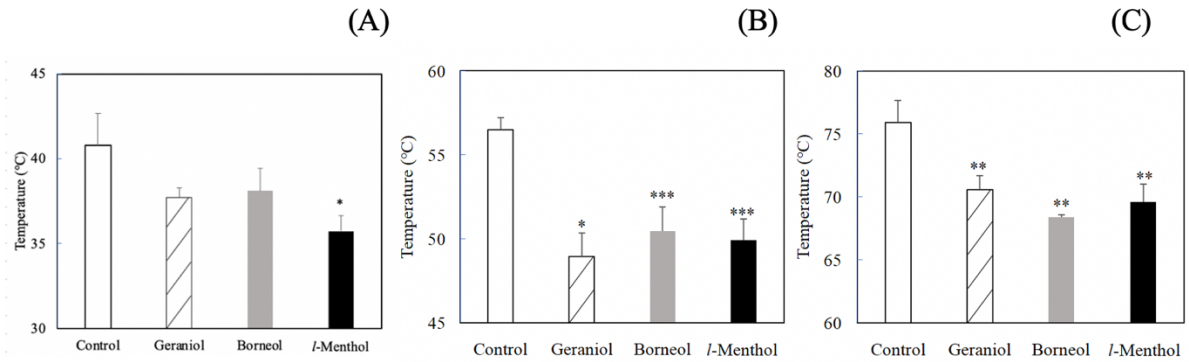

Fig. 5 Changes in the phase transition temperature of the hairless mouse SC treated with various terpenes. The phase transition temperatures were calculated from the DSC curves, around (A) 40 ℃, (B) 50 ℃, (C) 70 ℃. Each point represents the mean ± S.D. (n=3). * $p< 0.05$, ** $p< 0.01$, *** $p< 0.001$ vs. Control. Control was SC treated with IPA 30% formulation.

As mentioned above, three typical phase transitions occur for SC with increase in temperature that represent structural changes in the intercellular lipids in SC. In the DSC spectrum, all terpenes showed changes in the phase transition temperature. This suggests that chemical enhancers may directly act on intercellular lipids, resulting in distortion of the lipid structure, thereby changing the phase transition temperature to lower values. Moreover, *l*-menthol exhibited significant changes in all three typical phase transition temperatures, which revealed that *l*-menthol simultaneously relaxed both the packing structure and lamellar structure of the intercellular lipids. In contrast, geraniol at 40 ℃ did not show significant change compared with the control group, but a significant temperature drop was observed at 50 ℃, which indicated that geraniol had a greater influence on the lamellar structure than that of the other two terpenes. Borneol had less influence on temperature change compared with the other two terpenes; however, it showed a notable change at approximately 70 ℃. These results indicate that borneol had only slight effect on the lamellar structure and no influence

on the packing structure of SC. Collectively, *l*-menthol simultaneously relaxed the packing structure and lamellar structure of the intercellular lipids, whereas borneol had only slight influence on the lamellar structure. Differences in the extent of the effects of terpenes on the packing structure and lamellar structure might be attributed to different chemical structures of the terpenes.

3.4. Effects of terpenes on ATR-FTIR profile of SC

ATR-FTIR spectroscopy is considered a useful tool for determining the molecular vibrations of compounds in SC. This technique has been used to evaluate functional group interactions between skin penetration enhancers and intercellular lipids of SC. ATR-FTIR spectrum can be used to reveal the complex composition of SC, including lipids, proteins, minerals, and amino acids, through many infrared absorption bands [17]. Previous studies have shown that the peak near 2800–3000 cm^{-1} disappeared when the intercellular lipids of SC were extracted by a mixture of chloroform and methanol, indicating that the absorption peaks of CH_2 symmetric and asymmetric stretching vibrations are derived from intercellular lipids [49].

The mechanism of permeation enhancement of terpenes on transdermal delivery of FMT could be investigated through various spectral shifts. As shown in Fig. 6, main peaks appeared near 2800–3000 cm^{-1} infrared absorption spectra of hairless mouse skin after treatment with different terpenes.

Figure 6 shows two obvious peaks of asymmetric CH_2 stretching vibrations and symmetric CH_2 stretching vibrations at approximately 2920 cm^{-1} and 2850 cm^{-1}, respectively. It can be observed that all terpenes slightly shifted these two peaks to higher wavenumbers. In addition to the bands originating from the hydrophobic groups [$\nu_{as(CH2)}$ and $\nu_{s(CH2)}$], the bands

of CH_3 asymmetric stretching vibrations also revealed a simultaneous shift to a lower wavenumber and broadening for borneol and to a higher wavenumber for geraniol.

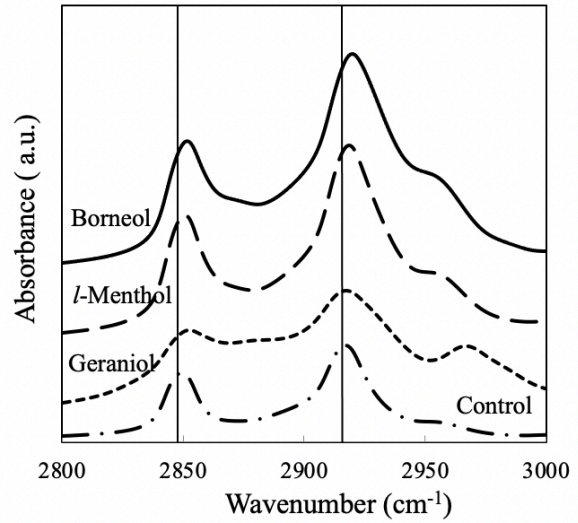

Fig. 6 ATR-FTIR spectra of hairless mouse after treatment with different terpenes.

Subsequently, the peak position, the wavenumber of the top of the peak, was calculated by subjecting the ATR-FTIR spectrum to the second derivative of the profiles, and then changes in the peak position of the CH_2 asymmetric stretching vibration were analyzed. As shown in Fig. 7, at 32 ℃, which represents the skin surface temperature, the CH_2 symmetric and asymmetric stretching vibration absorption peaks were shifted to a higher wavenumber, compared with the control group. At this temperature, *l*-menthol and borneol revealed a similar trend of wavenumber shifts, while geraniol showed slight difference compared the control group in asymmetric CH_2 stretching vibrations and the largest change in symmetric CH_2 stretching vibration. Fig. 8 shows a greater shift to a higher wavenumber by *l*-menthol and geraniol, whereas borneol exhibited a smaller shift to a higher wavenumber. Moreover, at a low temperature of 32 ℃, geraniol did not show a large shift to a higher wavenumber of the asymmetric CH_2 stretching vibration, but magnitude of the red shift of geraniol was obviously higher at high temperatures than that of the other two terpenes.

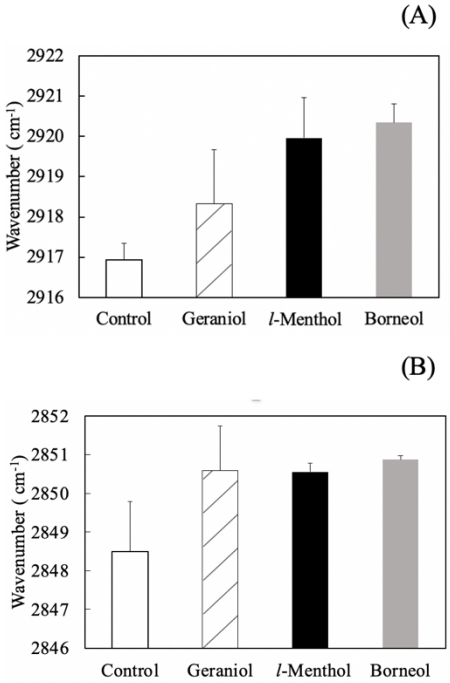

Fig. 7 The (A) asymmetric and (B) symmetric CH_2 absorption peak position of hairless mouse SC after treatment with control, geraniol, *l*-menthol, and borneol at 32°C. Each column represents the mean ± S.D. (n=3).

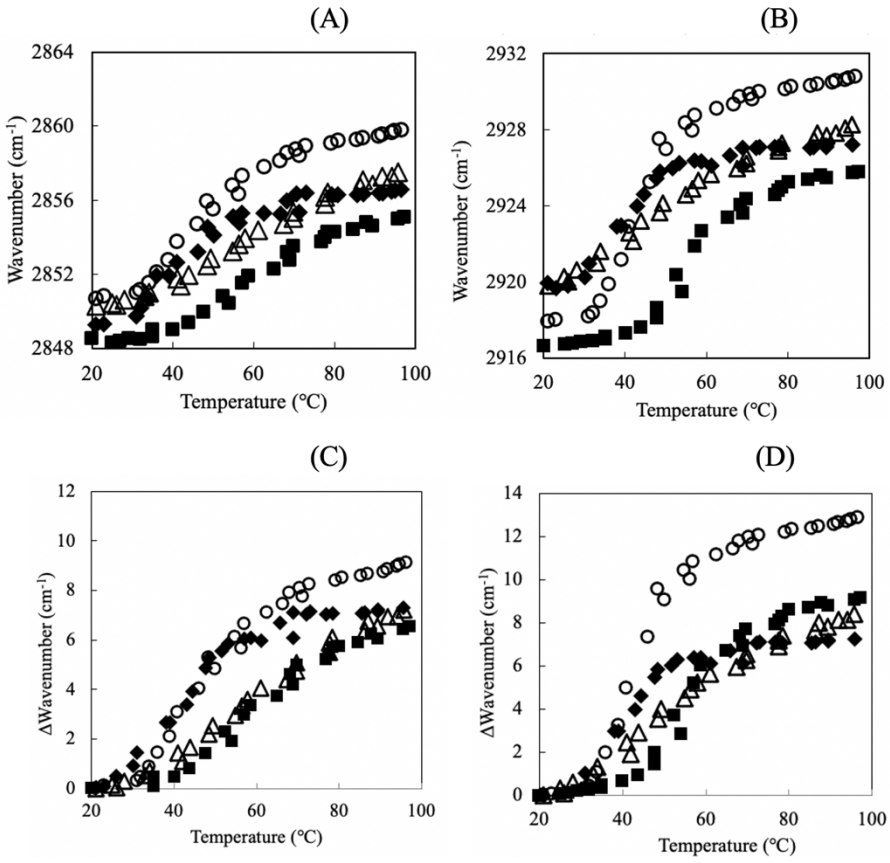

Fig. 8 Thermally induced changes in peak wavenumber of (A) asymmetric and (B) symmetric CH_2 stretching frequencies of intercellular lipids in the SC treated with various terpenes. The difference in wavenumber with blue shift of (C) asymmetric and (D) symmetric CH_2 stretching frequencies of intercellular lipids treated with various terpenes. Control is the SC treated by 30% IPA-solution. ◆: *l*-Menthol, △: Borneol, ○: Geraniol, ■: Control.

ATR-FTIR measurements can be used to observe changes in the fluidity of intercellular lipids after application of terpenes. ATR-FTIR spectra showed that all terpenes can increase the fluidity of intercellular lipids but had limited effect on keratinocytes. The result of Fig. 7 suggests that the fluidity of intercellular lipids may be increased at the skin surface temperature.

It is known that the absorption peaks of CH_2 symmetric and asymmetric stretching vibrations shift to a higher wavenumber with increase in temperature due to the increase in lipid fluidity. Because the shift of the C-H stretching frequency can be elucidated at the molecular level, the shift of the peak position to a higher wavenumber occurs when CH_2 groups along the alkyl chain of lipids change from the trans to the gauche conformation, indicating that the intercellular lipids in SC are disturbed. The extent of the shift in the C-H stretching vibrations is directly related to the ratio of trans to gauche conformers in the alkyl chain48). In this study, the wavenumber of the top of the peak (peak position) was calculated by subjecting the ATR-FTIR spectrum to the second derivative of the profiles, and then changes in the peak position of the CH_2 asymmetric stretching vibrations were analyzed. Figure 8 shows the shift in the peak position with increase in temperature in different terpene groups and the control group. These results indicated that the maximum wavenumber of the symmetric and asymmetric CH_2 stretching vibrations shifted to higher wavenumbers after the application of terpenes. In addition, shift of *l*-menthol and geraniol to higher wavenumber was observed; borneol also revealed a shift to a higher wavenumber here, but the magnitude of the shift was not large. Compared with the other groups, the magnitude of the red shift of geraniol was obviously higher at high temperatures, which might be due to the presence of unsaturated double bond in geraniol; however, further research is required.

For the typical symmetric CH_2 stretching vibration, geraniol exhibited the highest shift among the three terpenes, which might be attributed to the chemical structure of geraniol. In contrast to the other two terpenes, geraniol has a chain structure, which eases the lipid extraction compared with the ring structure. Furthermore, geraniol contains two unsaturated double bonds. This might make it perform better at high temperatures than the other two terpenes, but the specific mechanism requires further research.

In addition to the CH_2 symmetric and asymmetric peaks, a weak peak at 2960 cm^{-1} corresponding to the CH_3 asymmetric stretching vibration exists, as shown in Fig. 6, causing difference in the performance of the three terpenes. Borneol and *l*-menthol caused a slight shift to a lower wavenumber, whereas geraniol caused shift to a higher wavenumber. However, the bands of CH_3 vibrations originate not only from a specific component of SC, but from multiple components, including protein side chains, phospholipids, ceramides, and fatty acids 49). In addition, the bands of CH_3 vibrations overlapped with the bands of CH_2 vibrations with lower intensity. Therefore, further analysis based on these bands was not performed in this study.

3.5. FMT penetration enhancement effect of the three terpenes

The results of ATR-FTIR and DSC suggested that the terpenes had different degrees of effects on intercellular lipids to promote the skin permeation of drugs. Among them, *l*-menthol caused simultaneous relaxation of the packing structure and lamellar structure and increased the fluidity of the intercellular lipids of SC, thereby promoting FMT permeation. Geraniol showed a strong promoting effect on drug permeation, but it had only a slight effect on the packing structure and strong effect on the lamellar structure of intercellular lipids. In addition, geraniol had a longer effect of SC than other terpenes. Borneol had only a slight effect on the lamellar structure of intercellular lipids, and its promoting effect was not obvious.

Finally, based on the results of the present study, I have considered the dosage of FMT required for the treatment of GERD. The blood concentration of FMT for the treatment of GERD is still unclear. Therefore, I calculated the dosage of FMT applied for 24 hours based

on the maximum flux value obtained from our results and compared dosage of FMT administrated transdermally with the oral FMT dosage to determine whether our results are effective in treating GERD. Based on an oral dose of 20 mg twice per day and about 50% bioavailability for the clinical use of FMT in GERD, 20 mg needs to be absorbed transdermally to achieve the treatment of GERD. The highest flux of *l*-menthol and geraniol achieved in this study was 272.18 μg/cm^2/h and 112.56 μg/cm^2/h, respectively, and the cumulative amount of FMT which permeated from the gel (2 cm^2) was 2518.30 μg/cm^2 and 2919.52 μg/cm^2 at the final determination at 24h, respectively. Hence, transdermal FMT gel with an area of 3 cm^2 for *l*-menthol and 7cm^2 for geraniol would be sufficient for the management of GERD patients. Although the transdermal promotion effect of borneol on FMT was less pronounced compared to *l*-menthol and geraniol, the maximum flux of FMT when using borneol as a transdermal enhancer was 42 μg/cm^2/h. Therefore, transdermal FMT gel with an area of 19 cm^2 is also sufficient to meet the daily dosing needs of GERD patients. It is possible to use these terpenes as chemical enhancers for FMT transdermal gel.

Generally, human skin shows more resistance for drug permeation when compared to hairless mouse skin [50]. However, the significance of this study is that it supports the feasibility of developing a matrix-type TDDS for FMT that would increase patient compliance.

II. Transdermal absorption of a Flurbiprofen and Lidocaine complex in the non-crystalline form

1. Introduction

For the past half-century, researchers have been studying molecular complexes to improve the physicochemical characteristics of drugs, so as to improve the delivery efficiency of drugs in various formulations. Recently, amorphous drug formulations that exploit drug–drug interactions have been intensively studies [51]. Drugs in the amorphous state are generally in a higher energy state, making them more soluble in water than crystals. However, it has poor stability and usually transfers to crystals with a low energy state. Therefore, it is difficult to keep the drug substance stable in an amorphous state for a long time. In recent years, the amorphization of drugs by molecular complexing represented by co-amorphous [52], ILs [53], and DESs [54] has attracted attention for improving the physical properties of drugs and stabilizing them.

A co-amorphous system is a multi-component, single-phase amorphous solid system linked by weak intermolecular interactions between the components, such as hydrogen bonds of carboxylic acids, phenols/alcohols, and carboxamides [55]. ILs are formed from a combination of organic heterocyclic cations and organic or inorganic anions and are liquids at temperatures <100 °C [56]. In contrast, DESs are systems formed by eutectic mixtures of Lewis or Brønsted acids and bases, which contain various hydrogen bond acceptors and hydrogen bond donors [57, 58]. DESs are considered a new class of ILs analogs because they share many physical characteristics and properties but are two different types of solvents. The structure and properties of ILs and DESs are different. Ionic interactions dominate the behavior of ILs, and DESs, as a eutectic mixture of two or more different components, and they exhibit strong hydrogen bonding [59, 60]. With many suitable starting materials and their possible combinations, they can modify the properties of these substances for specific applications. Therefore, amorphous complexes can be used widely in science, research, and technology.

A TDDS can be used, alternatively, to minimize and avoid the limitations of the oral and parenteral administration of drugs [61]. However, the skin, as the largest tissue in the human body, is a barrier that limits the degree and speed of drug absorption by TDDS [62]. To

overcome these problems, ILs and DESs have emerged as medications with potential use as facilitators of dermal absorption [23, 28]. ILs and DESs can increase skin permeability by increasing the partition coefficient of the administered drug or its thermodynamic action and momentarily modifying the composition of the SC by breaking down the lipid structure [29-31]. Other enhancement mechanisms, such as decreased melting point and increased membrane solubility, are believed to be related to the permeation-enhancing capability of coformers such as menthol [32, 33]. Indeed, the oily liquid phase (active pharmaceutical ingredient DESs) containing a high drug concentration acts as a reservoir and thus may provide a higher driving force for the diffusion of drug molecules into the skin [34]. Some nonsteroidal anti-inflammatory drugs (NSAIDs) and lidocaine (LDC) are used as external preparations for analgesia and anti-inflammatory purposes. The complex formed by NSAIDs and LDC may change the physical and chemical properties, thereby improving skin penetration efficiency [16, 63, 64]. Therefore, it is necessary to investigate the effect of the prepared complexes on the transdermal ability of NSAIDs.

Indomethacin (IDM), which is a type of NSAIDs, exhibits anti-inflammatory and analgesic effects by suppressing the conversion of arachidonic acid to prostaglandins by inhibiting cyclooxygenase and suppressing prostaglandin synthesis. By inhibiting sodium channels in the nerve membrane, action potential conduction is reversibly suppressed, and sensory nerves and motor nerves are blocked [65]. Flurbiprofen (FLU) is also an NSAID used to treat the signs and symptoms of osteoarthritis and rheumatoid arthritis. FLU may also be used topically before ocular surgery to prevent or reduce intraoperative miosis. FLU is structurally and pharmacologically related to fenoprofen, ibuprofen, and ketoprofen [66]. With these NSAIDs, some researchers have used drug combinations to develop co-crystal systems to facilitate transdermal drug delivery [67]. Among them, local anesthetics are often used.

LDC is a local anesthetic and has applications in several superficial and invasive treatments. Since its discovery and availability for sale and use in the late 1940s, LDC has become a very commonly used medication [68]. Among the various routes of clinical use, some researchers have focused on the complex formed by NSAIDs and LDC because it can improve the bioavailability of the drug through routes such as the transdermal route [69]. DESs

has similar physical components and properties as ILs but possesses different chemical properties. The chemical structures of FLU and LDC are shown in Figure 9.

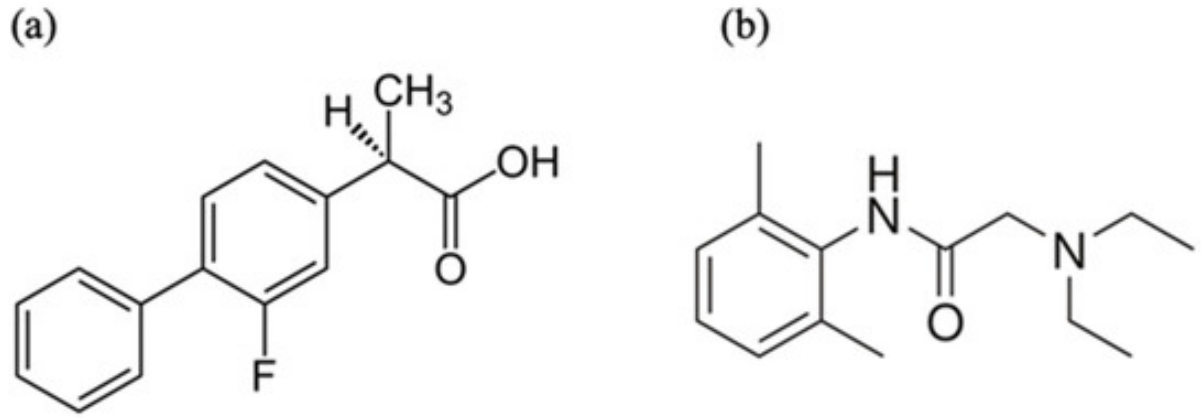

Figure 9. Chemical structures of the investigated molecules (a) flurbiprofen (FLU) and (b) lidocaine (LDC).

From the previous report, I obtained a reconstituted viscous paste from IDM and LDC, which is a local anesthetic ester in the form of liquids, creams, and gels used to relieve pain and discomfort. When kneaded with an appropriate amount of water, it was revealed that this paste is a molecular complex [70]. The skin permeation of IDM from the novel IDM/LDC complex was greater than IDM alone [71]. Until now, LDC has been proven to form a complex, or ILs with other NSAIDs. It have been reported the combinations with ibuprofen to form DES [72], naproxen to form IL [73], diclofenac to form IL [74], aceclofenac to form DES [75], and etodolac to form IL [76].

Therefore, I worked on forming an amorphous molecular complex in this study by combining various NSAIDs (FLU, etodolac, IDM, loxoprofen sodium, naproxen, and piroxicam) and LDC, and examined the physicochemical properties of the newly prepared complex. Hydroxypropyl methylcellulose (HPMC) hydrogel and white petrolatum as the base were selected to investigate the skin permeability of the obtained complex. The focus was on the transdermal delivery performance of NSAIDs, as well as the intermolecular interaction between an NSAID (FLU) and LDC, and the formation of a complex was confirmed using ATR-FTIR, thermal analysis, ^{13}C dipolar decoupling (^{13}C DD), ^{15}N cross-polarization (^{15}N CP), magic-angle spinning (MAS), and nuclear magnetic resonance (NMR) measurements. Finally, a novel transdermal system containing a complex of FLU and LDC for alleviating chronic pain and an inflammatory disease was developed.

2. Materials and methods

2.1. Materials

FLU was purchased from Tokyo Kasei Kogyo Co., Ltd. (Tokyo, Japan). Etodolac, IDM, loxoprofen sodium, naproxen, piroxicam, LDC (for biochemistry), and ethanol (special grade) were purchased from Wako Pure Chemical Industries, Ltd. (Osaka, Japan). As the base for the skin permeability test, a gel base prepared by hydroxypropyl methylcellulose (HPMC, ~15 mPa·S, 2% in H_2O (25 °C), Sigma-Aldrich Japan K.K., Tokyo, Japan) to 2 *w/w*% and white petrolatum (JP grade, Yoshida Pharmaceutical Co., Ltd., Tokyo, Japan) were used. A Franz-type diffusion cell (Osawa Shokai Co. Ltd., Tokyo, Japan) was used. Phosphate buffer solution (PBS, pH 7.4) was prepared from one tablet of PBS (Sigma-Aldrich Japan, Tokyo, Japan) dissolved in 200 mL water. All other reagents used were commercially available special-grade products.

2.2. Preparation of NSAIDs/LDC complexes

NSAIDs and LDC were weighed as 200 mg in total in a glass screwed vial. The molar ratio of NSAIDs and LDC is 1:1. The vial was then stirred using a vortex mixer for 5 min to obtain the physical mixture (PM). A small amount (about 800 μL) of ethanol was added to this PM, heated to 80 °C to dissolve, and kept at 40 °C for 12 h. Finally, it was dried under reduced pressure for 24 h, and a gel-like sample (defined as Complex) was obtained.

2.3. In vitro skin permeability test

The in vitro skin permeability test was performed with minor modifications in the methods previously reported 77, 78). The Complex was weighed with the concentration of FLU and LDC (1% *w/w*) and mixed with the HPMC gel using a pencil blender and with white petrolatum using an ointment plate and spatula, respectively. The skin permeation test gel sample with a total weight of 2 g was obtained. The preparations containing pure FLU and LDC were prepared the same way as the control group.

All animal experiments were carried out in accordance with the guidelines of the Institutional Animal Care and Use Committee (School of Pharmacy and Pharmaceutical

Sciences, Hoshi University, Tokyo, Japan). All procedures using animals were carried out according to protocols approved by the Animal Care and Use Committee of Hoshi University (approval number P21-076, 12 May 2021). Furthermore, all ARRIVE guidelines for the care and use of laboratory animals, the U.K. Animals (Scientific Procedures) Act, 1986 and associated guidelines, and the EU Directive 2010/63/EU for animal experiments were followed.

The excised skin of hairless mice (Labo Skin, HOS: HR-1 male, 7 weeks, Hoshino Laboratory Animals, Inc., Ibaraki, Japan) was mounted on a Franz-type diffusion cell (Vertical Diffusion Cell™, Hanson Research, Los Angeles, CA, USA). The donor cell was installed facing toward the SC side, and the receiver cell was forwarding the dermis side. Then, 7 mL phosphate buffer (pH 7.4), preheated to 32 °C, was added to the receiver cell. The prepared complex was applied to the donor cell (applicable area: 1.77 cm^2), containing 2 mg drug. Then, 0.5 mL of the receiver solution was collected at predetermined time intervals for 24 h, and each aliquot was replaced with 0.5 mL of fresh PBS to keep the volume of the receptor solution constant. The drug concentration in the collected solution was measured by HPLC, and the drug skin permeation rate (flux) and cumulative permeation amount were calculated from the obtained values.

2.4. Physicochemical properties of FLU/LDC complex

2.4.1. ATR-FTIR measurements

The infrared spectra were determined by the ATR method using an FTIR-4200 spectrometer (Jasco Co., Tokyo, Japan) and ATR unit (ATR PRO 670H-S, Jasco, Tokyo, Japan) with an internal reflection element (a diamond trapezoid having 45° entrance and exit faces). The detector used was a mercury cadmium telluride detector (MCT-4000M, Jasco, Tokyo, Japan). The spectra were acquired from 4000 to 400 cm^{-1} with a resolution of 4 cm^{-1} at 25 °C; each sample was scanned 64 times.

2.4.2. DSC measurements

DSC measurements were carried out using a Thermo plus EVO DSC 8230 (Rigaku, Tokyo, Japan) with a gas selector (Rigaku) and liquid nitrogen (LN_2) controller. An approximately 3–5 mg sample was weighed into the aluminum pan and sealed with the aluminum lid. Al_2O_3 was used as a reference. The measurement temperature was −100 °C–130 °C, with a temperature rise rate of 5 °C/min.

2.4.3. ^{13}C DD, ^{15}N CP, MAS, and NMR measurements

^{13}C DD/MAS and ^{15}N CP/MAS NMR measurements were recorded on an AVANCE III 600 spectrometer (Bruker Corporation, Billerica, MA, USA) with a frequency of 150.91 MHz for ^{13}C. The spectrometer was equipped with a 4.0 mm MAS probe head. The repetition delay time was 15 s; the MAS speed was 15 kHz for FLU and LDC and 5 kHz for the complex. Adamantane was used as an external standard (29.47 and 38.52 ppm, respectively).

2.5. Solubility test

FLU, LDC, PM, and the Complex were added in excess to 3 mL of water. The samples were shaken at a rate of 120 times/min for 24 h and the skin surface temperature of 32 °C. The suspension obtained after shaking was filtered through a polytetrafluoroethylene membrane filter (0.45 μm), and the filtrate was appropriately diluted to prepare a sample solution. The drug concentration in the sample solution was calculated by the high-performance liquid chromatography (HPLC) method.

2.6. HPLC measurements

The HPLC equipment of ChromNAV Chromatography Data System, with an autosampler (AS-2055plus), pump (PU-2080plus), ultraviolet-visible detector (UV-2075plus), column oven (CO-2060plus), and solvent deaerator (DG-2080-53), manufactured by Jasco Corporation (Tokyo, Japan), was used. The mobile phase comprised a phosphate buffer at pH 5.9: acetonitrile = 65:35, and the stationary phase was an Inertsil® ODS-3 (4.6 × 150 mm, 5 μm, GL Sciences Co., Ltd., Tokyo, Japan). The measurement conditions were 40 °C for the column oven, 1 mL/min for the flow rate, 20 μL for the injection volume, and 254 nm for the

measurement wavelength. Phosphate buffer pH 5.9 was prepared by dissolving 6.8 g of potassium dihydrogen phosphate in 800 mL of water, adding diluted potassium hydroxide (0.1 g/mL) to adjust the pH to 5.9, and then adding water to 1000 mL.

2.7. Data analysis of in vitro skin permeability test

The cumulative amount of drug permeated through the skin was plotted as a function of time. Subsequently, the flux was calculated from the slope of the linear region of this plot and expressed as (μg/cm^2/h). The lag time (h) was determined by finding the linear portion of the cumulative amount versus time plot and extrapolating back to the *x*-axis.

3. Results and discussions

3.1. Amorphous molecular complex formation screening between NSAIDs and LDC

Amorphous molecular complexes of various NSAIDs and LDC were prepared by the method described above. Comparing the appearance with each other, it was obvious that the FLU/LDC, etodolac/LDC, IDM/LDC, and naproxen/LDC complexes developed a gel-like liquid state at room temperature. However, the Lox/LDC and Pir/LDC complexes developed a hard crystalline state at room temperature. From these complexes, IDM/LDC and Pir/LDC complexes were yellow, the Lox/LDC complex was white, and other complexes were transparent. It has already been reported that the etodolac/LDC complex was an IL [76] and the IDM/LDC complex was reported to form a water-soluble complex as described previously [70]. On the other hand, the naproxen/LDC complex was judged not to be a molecular complex because no interaction with LDC was observed according to our method as a result of the preliminary test. However, Fiandaca et al. reported that naproxen and LDC form an IL material at a peritectic point corresponding to 2 mol of naproxen to 1 mol of LDC [73]. The method described in the study by Fiandaca et al. used tetrahydrofuran to prepare IL, whereas I used ethanol, which could have led to different results.

On the other hand, the interaction was confirmed from the preliminary test results regarding the gel-like mixture formed by the combination of FLU and LDC. Few reports of amorphous complex of FLU and LDC for a novel transdermal system and their interaction

mechanisms have been shown. For defining it as co-amorphous, IL, or DES, detailed physicochemical properties of the gel-like compound was subsequently analyzed.

3.2. Solubility test

Figure 10 shows a comparison of the solubility of the FLU/LDC Complex, pure drug, and PM at 32 °C. FLU is almost insoluble in water, whereas LDC is soluble in water. The solubility of FLU in the Complex was about 10.0 mg/mL, which was about 100 times higher than that of the pure drug at 0.1 mg/mL. The solubility of FLU in PM was 4.8 mg/mL, which was about half that of the Complex. However, the solubility of LDC was 11.5 mg/mL, which was about twice as high as that of the pure drug. The solubility of LDC in PM was 4.5 mg/mL, which was about 40% of that of the Complex. Thus, the PM and the amorphous complex increased the solubility of FLU and LDC. However, the amorphous complex significantly contributed to the increased drug solubility more so than the PM.

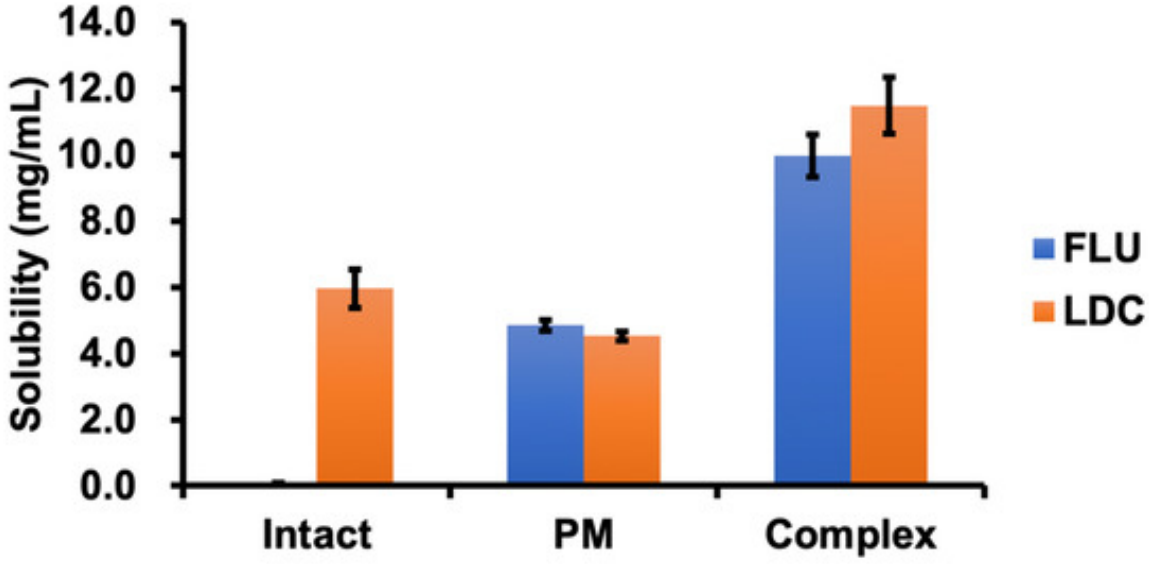

Figure 10. Solubility of FLU and LDC from the Complex at 32 °C. Each column represents the mean ± S.D. (n=3).

This result was consistent with the previous report [76]. The formation of an amorphous state would reduce the melting point and thus increase the solubility in water. On the other hand, the presence of the amorphous complex in the ionized form increased the potential for the establishment of hydrogen bonds and hydration, thus allowing the drug to achieve higher solubility. Interestingly, the solubility of LDC in PM was slightly less than that of the LDC

alone, but its solubility in the Complex was twice compared with that of the LDC alone. These outcomes suggest that the structure of the amorphous complex significantly increased the hydrophilicity of FLU and LDC. A comparison between the two compositions, FLU and LDC, showed that FLU exhibited significantly better solubility improvement than LDC, suggesting that the interaction between LDC and FLU in the Complex was more effective in promoting the solubility of FLU.

3.3. Skin permeation test of FLU/LDC complex

In Japan, several transdermal formulations of FLU are commercially available for their analgesic, anti-inflammatory, and antipyretic properties. Moreover, S-flurbiprofen (S-FLU) plaster, which contains the primary active NSAID S-FLU, was launched in 2016. S-FLU is highly skin permeable and reaches a significantly higher concentration in the synovium than topical FLU [79]. Additionally, the clinical combined therapeutic effects of LDC and FLU for reducing pain were enhanced [80]. Therefore, the clinical application of a transdermal formulation containing FLU and LDC would be crucial.

Skin permeation amounts of FLU (Figure 11a) and LDC (Figure 11b) are shown with 2% HPMC gel used as the base. The amount of FLU permeated when white petrolatum was used as the base is shown in Figure 11c, and the amount of LDC permeated is shown in Figure11d.

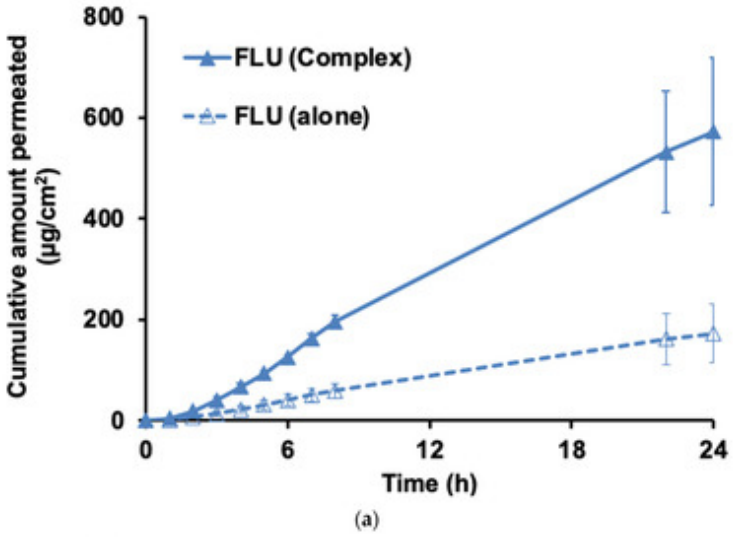

(a)

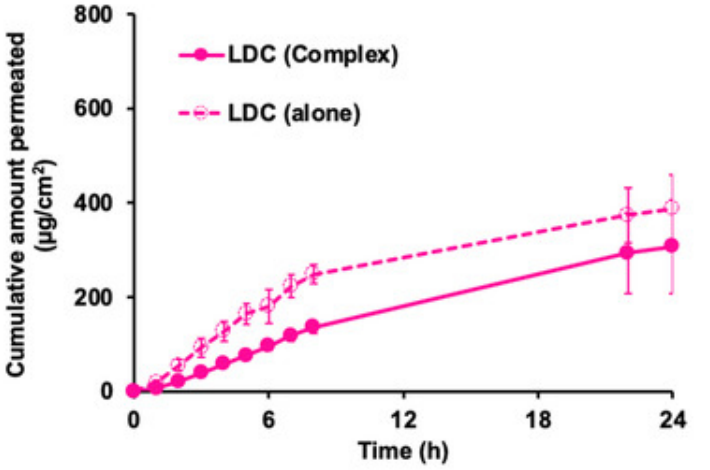

(b)

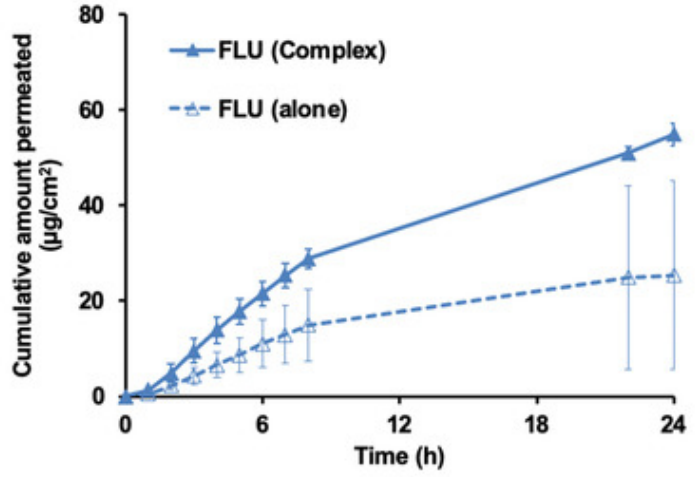

(c)

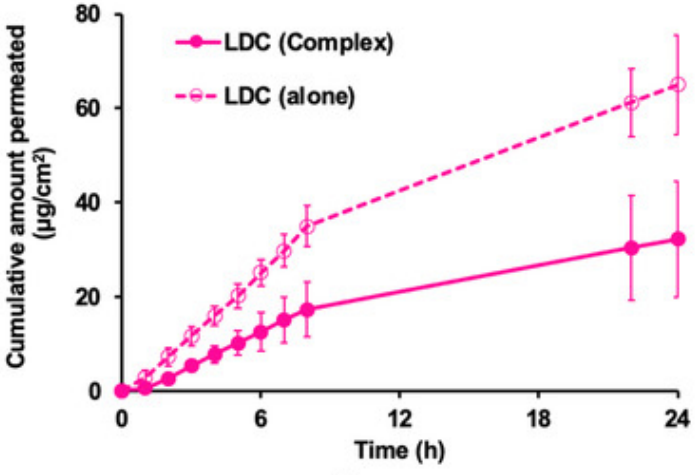

(d)

Figure 11. Skin permeation profile of FLU and LDC from the Complex in 2% HPMC gel (a,b) and white petrolatum (c,d). Each column represents the mean ± S.D. (n=3).

Figure 11a demonstrates that when 2% HPMC gel was used as a base, the FLU alone flux was 8.0 μg/cm^2/h, whereas that for the FLU from the Complex was 30.1 μg/cm^2/h, with an increase of about 3.8 times (Figure 11a). On the other hand, the flux of LDC from the Complex was about 1/2 that of LDC alone (18.4 μg/cm^2/h) (Figure 11b), i.e., FLU in the Complex had a better permeability than FLU alone, whereas the LDC in the Complex could not be permeated through the skin as much as from the LDC alone. From this, it was found that the combined use of LDC improved the skin permeability of FLU.

When white petrolatum was used, the flux of FLU from the complex was 4.32 μg/cm^2/h, which was about twice the flux from the FLU alone (Figure 11c), and for the LDC, it was similar to that with 2% HPMC gel. In the case of the Complex, the flux was 2.5 μg/cm^2/h, about 50% lower than that of the LDC alone, 4.46 μg/cm^2/h (Figure 11d). It was speculated that the flux of FLU increased when using the Complex because the solubility was increased by interacting with LDC. This drug–drug interaction may also affect the structure of the SC to improve FLU permeability. On the other hand, the reason why the permeability of LDC from the Complex decreased compared with that of the pure drug is unclear, despite the fact that LDC has high skin permeability. Miwa et al. reported that when comparing the skin permeation of LDC formed as IL with etodolac (1:1, mol/mol) and LDC alone in a transdermal patch through the Yucatane Micro Pig, LDC alone showed a higher flux than LDC formed as IL 76). They suggested that LDC–etodolac IL in the patch appeared to be able to self-sacrificially improve the limiting steps, thereby improving the skin permeation of etodolac through the matrix and SC of the skin and that both drugs might stay together in the skin as ion pairs or clusters rather than as independent solvated ions. However, the underlying mechanism behind the improved skin permeation was not clear [76)]. I hypothesized that the reason for the decreased skin permeability of LDC from the Complex was consistent with their findings.

Finally, I compared the drug skin permeability of the complexes on different bases. I observed that during the initial 8 h, LDC alone exhibited better skin permeability in both bases (Figure 11b, d), followed by FLU in the Complex (Figure 11a, c). However, with time, the FLU in the Complex showed better skin permeability than the LDC alone in a 2% HPMC gel base. In both bases, the skin permeability of FLU in the Complex was greater than that of

FLU alone, indicating that LDC could promote the skin permeation ability of FLU. The difference was that the cumulative amount of FLU from the Complex in the 2% HPMC gel was about six times that from FLU alone. In contrast, the cumulative amount of FLU from the Complex in the white petrolatum was only about three times that from FLU alone. When the 2% HPMC gel was used, the cumulative amount of the four samples was much greater than that with the white petrolatum base. Thus, the distribution to the skin was reduced in the white petrolatum base, and the FLU permeability was also reduced. This might be caused by the different solubilities of the drugs LDC and FLU in the two bases.

3.4. Physicochemical properties of FLU/LDC complex

To explore the physical and chemical properties of the FLU/LDC complex (Complex), I performed ATR-FTIR, DSC, and MAS/NMR measurements on the Complex and compared it with the pure drug to clarify the changes in its physical and chemical properties.

3.4.1. ATR-FTIR measurements

Figure 12 shows the results of ATR-FTIR measurements for the FLU, LDC, PM, and the Complex. ATR-FTIR spectroscopy has been considered a useful tool for determining molecular complex formation. For the FLU, the stretching vibrations of the carboxylic acid carbonyl group were detected at 1695 cm^{-1}. The amide carbonyl stretching vibrations for the LDC were recorded at 1661 cm^{-1}. This recorded FTIR spectrum and band assignment correlate with the previous reports [66, 73, 81, 82].

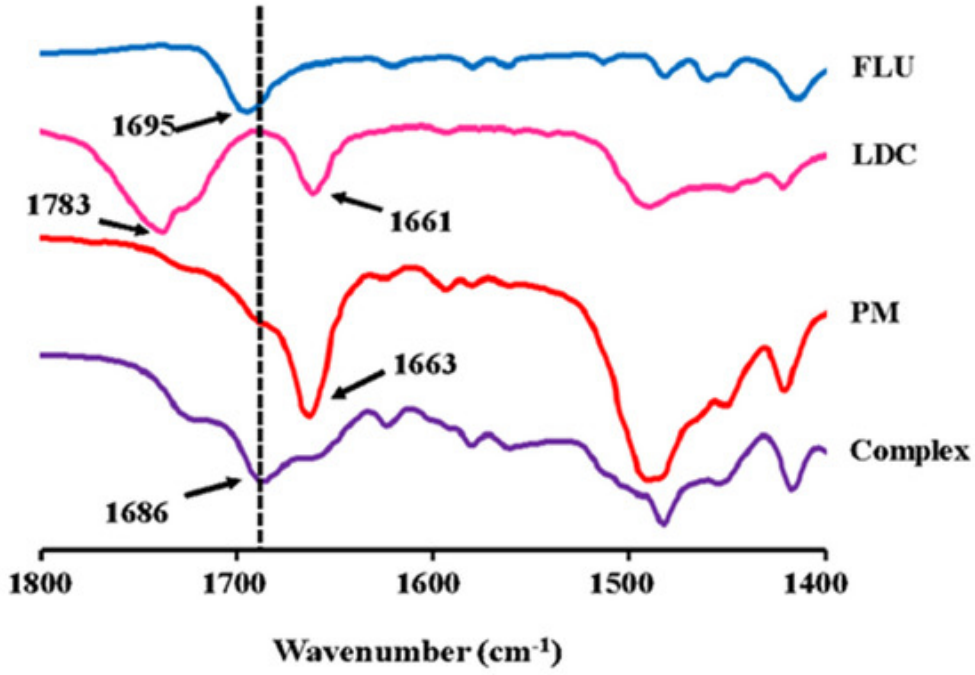

Figure 12. ATR-FTIR spectrum for the FLU, LDC, PM, and FLU/LDC complex.

In the Complex, the peaks of 1695 cm^{-1} derived from the carboxy group observed in FLU and 1783 and 1663 cm^{-1} derived from amide I observed in LDC can be seen faintly, covered by a larger peak at 1686 cm^{-1}. All these peaks disappeared in the PM sample. The Complex sample had a peak shift to 1686 cm^{-1} that differed from that in pure FLU, LDC, and PM samples. These results were consistent with the previous studies of the combination between other NSAIDs and LDC [75, 76]. The change in the electron density of FLU molecules after the complex formation could explain the peak shift. These spectrum changes suggested a hydrogen bond formed between FLU and LDC in the complex sample. Because only the peak shift had occurred and no new peaks appeared, it also reflected that a hydrogen bond may have formed between LDC and FLU, and there was no clear sign of ionization or proton transfer. Recently, Agarwal et al. reported that a eutectic formation was obtained by combining LDC and myristic acid at a molar ratio of 1:1 because of a loss in the dimeric conformation of myristic acid, resulting in hydrogen bonding of its −COOH group with amide I moieties of LDC [83]. Furthermore, a frequency of 1664 cm^{-1} for the amide C=O stretching mode in pure LDC is typical for hydrogen-bonded amide carbonyls. This band decreases in intensity in the binary mixtures with increasing myristic acid. I speculate that these observations indicate that the intermolecular hydrogen bonding between the amide −C−O and

−N−H of neighboring molecules within LDC is reduced or lost in the binary mixtures with myristic acid and is replaced by hydrogen bonding between −N−H of the LDC and −C=O of myristic acid and also −C=O of the LDC with myristic acid −OH. These observations suggest that the intra- and intermolecular hydrogen bonding within myristic acid alone, as well as the intermolecular hydrogen bonding within LDC alone, are each replaced by weaker intermolecular bonds formed between LDC and myristic acid in the binary mixtures, which explains the relatively lower melting point of the binary mixtures in comparison with that of LDC alone and myristic acid, respectively [83]. Consequently, it could be inferred that a relatively weak hydrogen bond is formed between the carboxyl group of FLU and the amide group of LDC.

3.4.2. DSC measurements

Figure 13 shows the results of the DSC measurement of FLU, LDC, PM, and the Complex. The melting point was confirmed at about 115 °C for FLU and about 68 °C for LDC, which correlated with the published data [82]. In the PM sample, an endothermic peak considered a co-melting point was observed at about 38 °C. On the other hand, no clear endothermic peak was observed for the Complex sample in the measured temperature range, suggesting that the Complex had no melting transition and was in an amorphous state. In the Complex, a baseline change was observed at about −18 °C, indicating that glass transition may have occurred before and after this temperature. Combined with the FTIR results, all these changes proved that the developed system can be considered a eutectic system and that the Complex had formed an amorphous state.

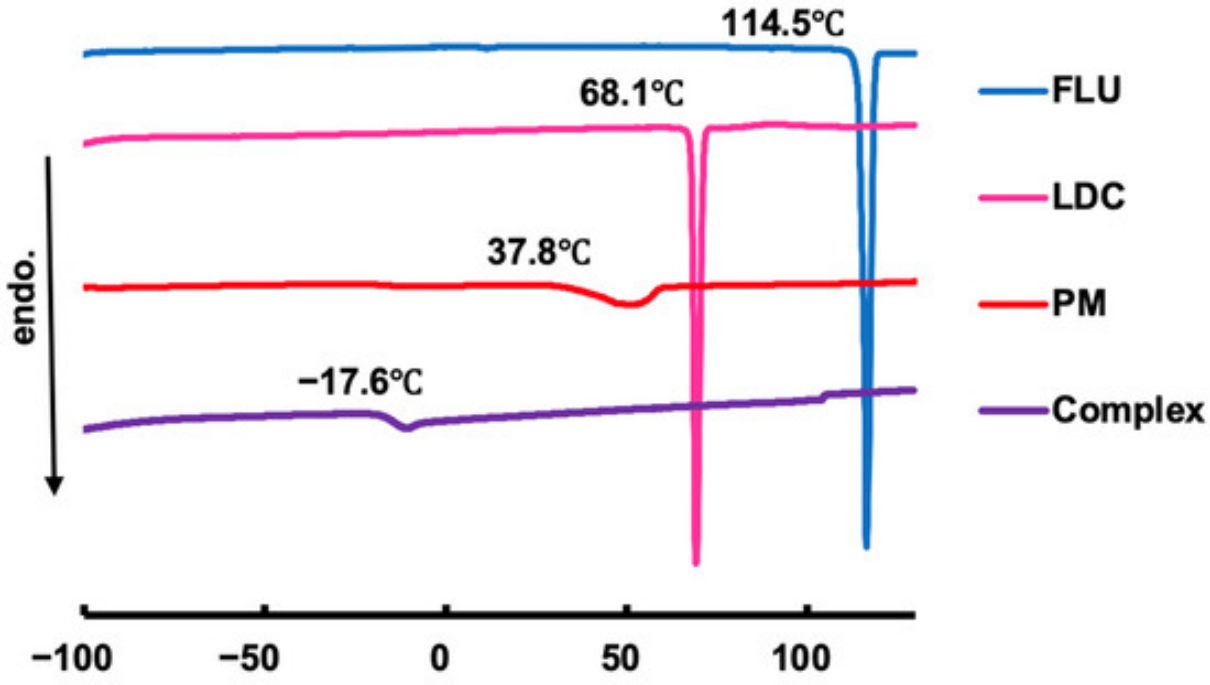

Figure 13. DSC profiles for the FLU, LDC, PM, and FLU/LDC complex.

3.4.3. ^{13}C DD and ^{15}N CP/MAS NMR measurements

MAS NMR enables the study of ILs and DESs over a wide range of temperatures and their characterization in liquid and solid states in a single setup. There are a very limited number of previous MAS NMR studies on ILs or DESs; these have focused on solutes dissolved in the IL or DES or interactions of the IL or DES with other materials or biological molecules rather than directly probing intermolecular interactions between the molecules of the neat ILs or DESs themselves [84-86]. Therefore, the ^{13}C DD/MAS NMR experiment was used to investigate the interaction between FLU and LDC in the complex. The NMR spectra of FLU, LDC, and the Complex are shown in Figure 14. In the Complex, the signals at 11.0 and 159 ppm were observed, which were not observed in pure FLU and LDC. The peak derived from the carbon at position a, which forms the carboxy group of FLU, was observed at around 184 ppm in pure FLU, whereas it was shifted to about 178 ppm in the Complex. The peak derived from the aromatic ring, observed at around 110–140 ppm in the FLU and LDC alone, was broadened in the Complex.

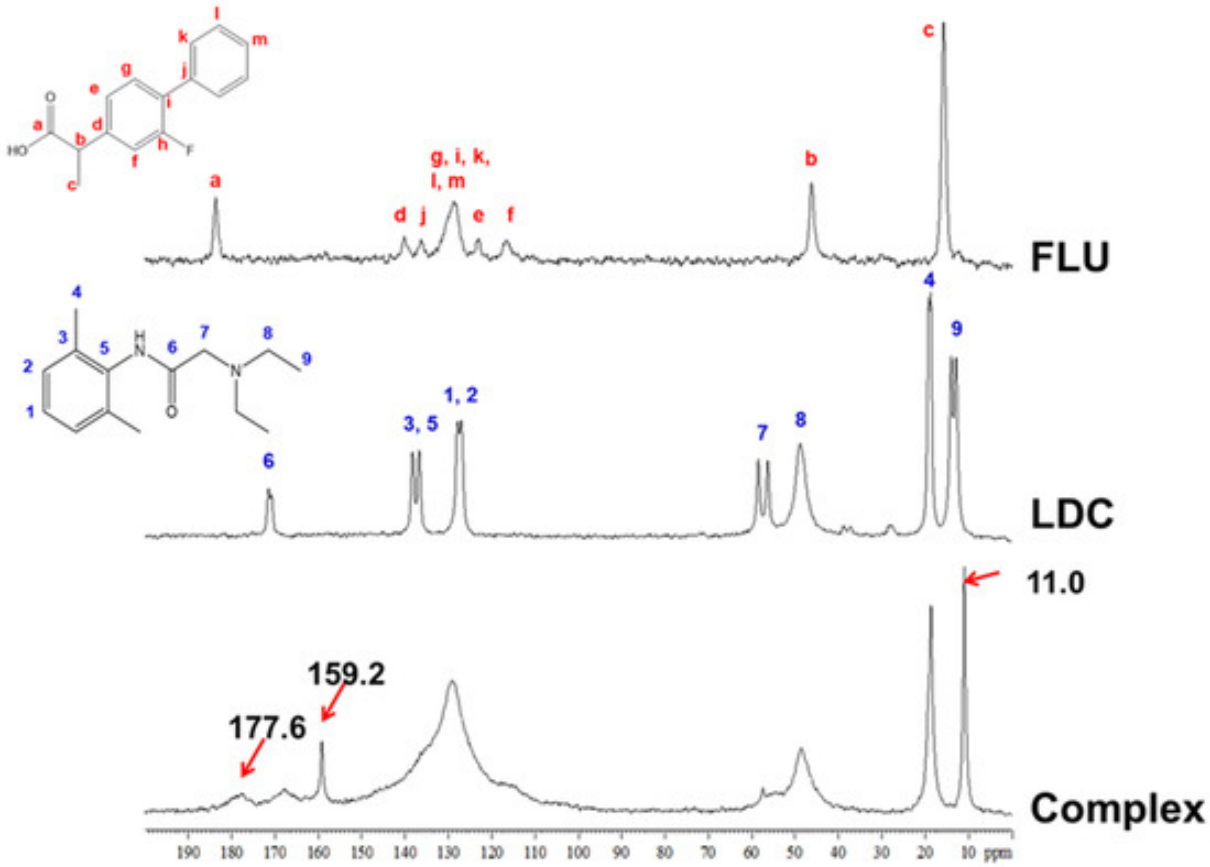

Figure 14. ^{13}C DD/MAS NMR spectra of FLU, LDC, and FLU/LDC complex.

Figure 15 shows the results of ^{15}N CP/MAS NMR measurements that were performed to observe the nitrogen signals of the LDC alone and in the Complex. The results showed that the signal position of tertiary amine in the Complex was shifted to a much higher field (−340.9 ppm to −332.2 ppm) than that in LDC alone, suggesting that the carboxyl group of FLU interacted with the tertiary amine of LDC.

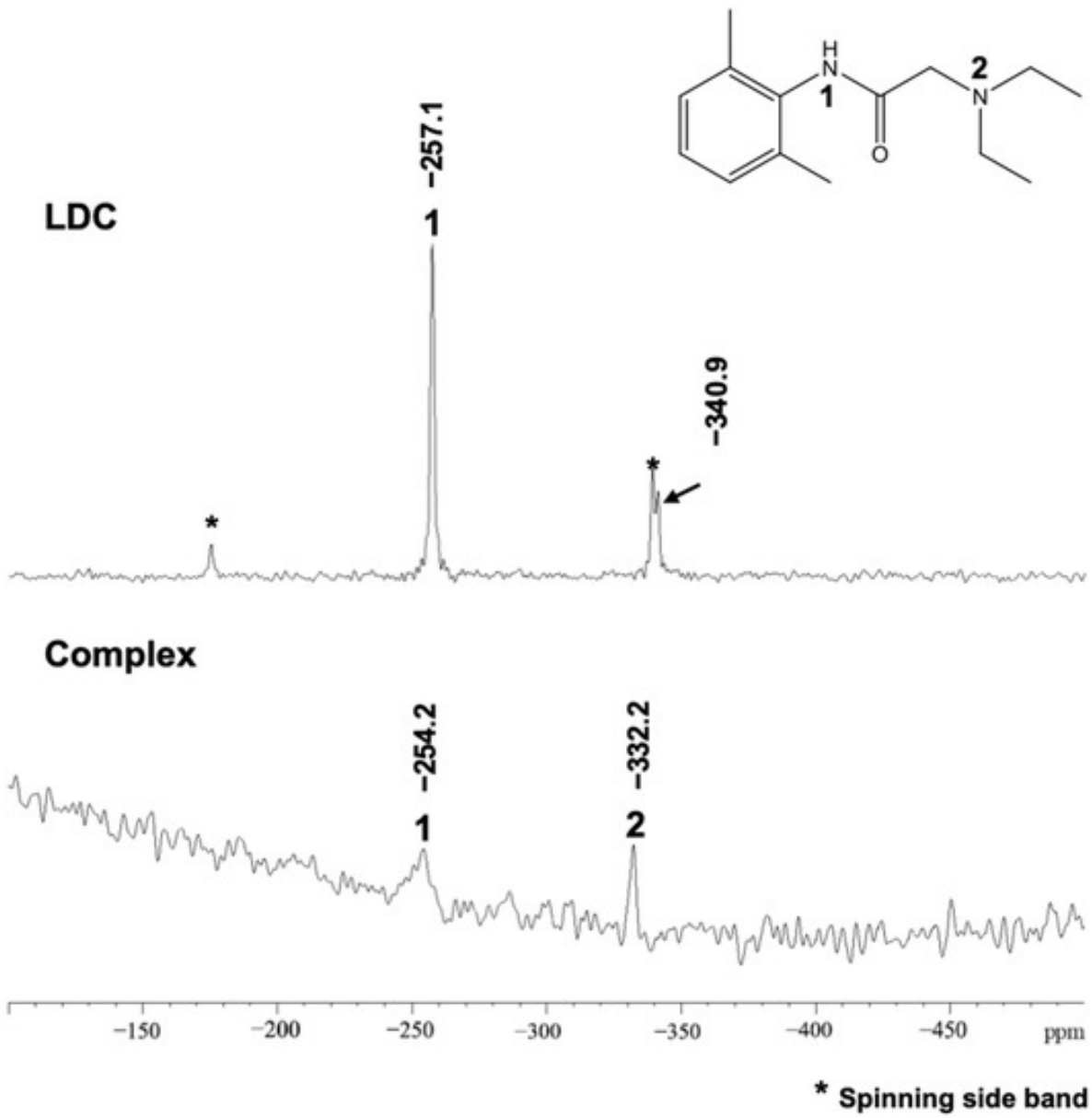

Figure 15. ^{15}N CP/MAS NMR spectra of FLU, LDC, and FLU/LDC complex.

From these results, it was suggested that not only the ionic interaction between the carboxyl group of FLU and the secondary amine of LDC but also the Π-Π interaction between the aromatic rings of FLU and LDC contributed to the molecular complex formation. Moreover, ATR-FTIR measurements suggested that the carboxyl group of FLU and the amide group of LDC form a relatively weak hydrogen bond. Therefore, it was difficult to clearly define the complex composed of FLU and LDC as IL or DES. The complex was categorized within a boundary between DES and partially ionized ILs [87].

Conclusions

Both ways mainly studied in this work are effective in increasing the transdermal penetration of specific insoluble drugs.

For the chemical enhancer terpenes, all the three terpenes increase the fluidity of the intercellular lipids and improve the permeability of the FMT through SC. However, terpenes may have different degrees of effect on the packing structure and lamellar structure of intercellular lipids in SC, which was dependent on the type of terpenes. The maximum flux of FMT was increased by the administration of terpenes, which indicates terpenes are effective chemical enhancers to promote FMT penetrability through the skin; however, among the administered terpenes, geraniol was the most effective. The penetration mechanism of terpenes may include interaction with the lipids in SC to increase the fluidity of the rigid barrier, thereby increasing skin permeation of the drug. Geraniol had great influence on the lamella structure of the SC, which might be the main mechanism influencing permeation of FMT through the skin.

For changing the nature of API by ILs, I successfully obtained a gel-like mixture at room temperature by mixing FLU and LDC with ethanol from the screening of the amorphous molecular complex formation between NSAIDs and LDC. The results of ATR-FTIR, DSC, and MAS/NMR measurements proved that a molecular complex in an amorphous state was formed, and I defined the Complex as IL and/or DES. Using the complex of FLU and LDC, it was found that the solubility of FLU and LDC was increased about 100 and 2 times compared with the drug alone, respectively. It was clarified that the skin permeability of FLU from the HPMC gel and white petrolatum containing the Complex was significantly improved compared with the FLU alone, which indicated that LDC could interact with FLU to improve its ability to permeate through the skin.

Overall, TDDS offers compelling opportunities to address the low bioavailability of many oral drugs, the pain and inconvenience of injections, and the limited controlled-release options of both. And both the ways in this study have great potential to be used in transdermal formulation, to improve the permeation of water insoluble drugs through the skin.

Acknowledgements

Upon the completion of this thesis, I am grateful to those who had offered me encouragement and support during the course of my study.

First of all, the profound gratitude should go to my supervisor, Professor Yonemochi Etsuo and Dr. Furuishi Takayuki. They had given me great instructions and encouragements during the process of selecting the research topic, carrying out the experiments, writing the thesis and correcting the grammatical errors. They had given me a lot of insightful comments, which provided me with many enlightening ideas, and inspiring me to a great extent. I do appreciate their patience, encouragement both in my study and in my life. I am also greatly indebted to Professor Obata Yasuko. In the preparation of one of my publications, her willingness to give me her time so generously has been much appreciated. Her tremendous assistance in developing the framework for analysis and in having gone through the draft versions of the manuscript several times deserve more thanks than I can find words to express. It can be said that without their help, the thesis could not be finished.

Also, I would like to extent my sincere gratitude to all the professors who had taught me and gave me advice before. The wonderful courses greatly broadened my horizon and enriched my knowledge, which made me a more comprehensive and mature individual.

Special thanks should go to all the students in Department of Physical Chemistry. As a foreign student, I was not familiar with the experimental instructions and operations at first. They had offered me warm help in my study and in my life as well. I am really grateful that they had given me some precious comments and help me to solve the problems during my study.

Last but not least, I would like to express my thanks to my beloved parents for their unfailing love and support. For so many years, they have always been supporting me and respecting me. Their love and care are the greatest fortune of my life.

References

1)Shi Y., Zhao Z., Gao Y., Pan D. C., Salinas A. K., Tanner E. E. L., Guo J. and Mitragotri S., Oral delivery of sorafenib through spontaneous formation of ionic liquid nanocomplexes, J Control Release, 322, 602-609(2020).

2)Sintra T. E., Abranches D. O., Benfica J., Soares B. P., Ventura S. P. M. and Coutinho J. A. P., Cholinium-based ionic liquids as bioinspired hydrotropes to tackle solubility challenges in drug formulation, Eur J Pharm Biopharm, 164, 86-92(2021).

3)Zhang Y., Yu J., Kahkoska A. R., Wang J., Buse J. B. and Gu Z., Advances in transdermal insulin delivery, Adv Drug Deliv Rev, 139, 51-70(2019).

4)Takahashi C., Hattori Y., Yagi S., Murai T., Takai C., Ogawa N., Tanemura M., Fuji M., Kawashima Y. and Yamamoto H., Optimization of ionic liquid-incorporated PLGA nanoparticles for treatment of biofilm infections, Mater Sci Eng C Mater Biol Appl, 97, 78-83(2019).

5)Wu X., Zhang H., He S., Yu Q., Lu Y., Wu W., Ding N., Zhu Q., Chen Z., Ma Y. and Qi J., Improving dermal delivery of hyaluronic acid by ionic liquids for attenuating skin dehydration, Int J Biol Macromol, 150, 528-535(2020).

6)Abednejad A., Ghaee A., Morais E. S., Sharma M., Neves B. M., Freire M. G., Nourmohammadi J. and Mehrizi A. A., Polyvinylidene fluoride-Hyaluronic acid wound dressing comprised of ionic liquids for controlled drug delivery and dual therapeutic behavior, Acta Biomater, 100, 142-157(2019).

7)Giri T. K., Chakrabarty S. and Ghosh B., Transdermal reverse iontophoresis: A novel technique for therapeutic drug monitoring, J Control Release, 246, 30-38(2017).

8)Li Y., Yang J., Zheng Y., Ye R., Liu B., Huang Y., Zhou W. and Jiang L., Iontophoresis-driven porous microneedle array patch for active transdermal drug delivery, Acta Biomater, 121, 349-358(2021).

9)Dobler D., Schmidts T., Klingenhofer I. and Runkel F., Ionic liquids as ingredients in topical drug delivery systems, Int J Pharm, 441, 620-627(2013).

10)Moniruzzaman M., Kamiya N. and Goto M., Ionic liquid based microemulsion with pharmaceutically accepted components: Formulation and potential applications, J Colloid Interface Sci, 352, 136-142(2010).

11)Prausnitz M. R. and Langer R., Transdermal drug delivery, Nat Biotechnol, 26, 1261-1268(2008).
12)Millington P. F., Skin / P.F. Millington, R. Wilkinson, Cambridge University Press, (1983).
13)Waters C., The development of the rotigotine transdermal patch: a historical perspective, Neurol Clin, 31, S37-50(2013).
14)Yang C., Guo S., Wu X., Yang P., Han L., Dai X. and Shi X., Multiscale study on the enhancing effect and mechanism of borneolum on transdermal permeation of drugs with different log P values and molecular sizes, Int J Pharm, 580, 119225(2020).
15)Bolzinger M.-A., Briançon S., Pelletier J. and Chevalier Y., Penetration of drugs through skin, a complex rate-controlling membrane, Curr Opin in Colloid & Interface Sci, 17, 156-165(2012).
16)Marjukka Suhonen T., Bouwstra J. A. and Urtti A., Chemical enhancement of percutaneous absorption in relation to stratum corneum structural alterations, J Control Release, 59, 149-161(1999).
17)Chantasart D. and Li S. K., Structure Enhancement Relationship of Chemical Penetration Enhancers in Drug Transport across the Stratum Corneum, Pharmaceutics, 4, 71-92(2012).
18)Yang Y., Xu L., Jiang D., Chen B. Z., Luo R., Liu Z., Qu X., Wang C., Shan Y., Cui Y., Zheng H., Wang Z., Wang Z. L., Guo X. D. and Li Z., Self-Powered Controllable Transdermal Drug Delivery System, Adv Funct Mater, 31, 2104092(2021).
19)Karande P., Jain A. and Mitragotri S., Discovery of transdermal penetration enhancers by high-throughput screening, Nat Biotechnol, 22, 192-197(2004).
20)Denet A. R., Vanbever R. and Preat V., Skin electroporation for transdermal and topical delivery, Adv Drug Deliv Rev, 56, 659-674(2004).
21)Ogura M., Paliwal S. and Mitragotri S., Low-frequency sonophoresis: current status and future prospects, Adv Drug Deliv Rev, 60, 1218-1223(2008).
22)Prausnitz M. R., Gill H. S. and Park J.-H., Microneedles for drug delivery, CRC Press, 323-338 (2008).
23)Lu B., Liu T., Wang H., Wu C., Chen H., Liu Z. and Zhang J., Ionic liquid transdermal delivery system: Progress, prospects, and challenges, J Mol Liq, 351, 118643(2022).
24)Aqil M., Ahad A Fau - Sultana Y., Sultana Y Fau - Ali A. and Ali A., Status of terpenes as skin penetration enhancers, Drug Discov Today, 12(23-24), 1061-1067(2007).
25)Sapra B., Jain S. and Tiwary A. K., Percutaneous permeation enhancement by terpenes: mechanistic view, AAPS J, 10, 120-132(2008).

26)Berlin M., Przyklenk K. H., Richtberg A., Baumann W. and Dressman J. B., Prediction of oral absorption of cinnarizine--a highly supersaturating poorly soluble weak base with borderline permeability, Eur J Pharm Biopharm, 88, 795-806(2014).
27)Anjos J. L., Neto Dde S. and Alonso A., Effects of 1,8-cineole on the dynamics of lipids and proteins of stratum corneum, Int J Pharm, 345, 81-87(2007).
28)Al-Akayleh F., Adwan S., Khanfar M., Idkaidek N. and Al-Remawi M., A Novel Eutectic-Based Transdermal Delivery System for Risperidone, AAPS PharmSciTech, 22, 4(2020).
29)Campos W. F., Silva E. C., Oliveira T. J., Oliveira J. M., Jr., Tubino M., Pereira C., Vila M. M. and Balcao V. M., Transdermal permeation of bacteriophage particles by choline oleate: potential for treatment of soft-tissue infections, Future Microbiol, 15, 881-896(2020).
30)Jorge L. R., Harada L. K., Silva E. C., Campos W. F., Moreli F. C., Shimamoto G., Pereira J. F. B., Oliveira J. M., Jr., Tubino M., Vila M. and Balcao V. M., Non-invasive Transdermal Delivery of Human Insulin Using Ionic Liquids: In vitro Studies, Front Pharmacol, 11, 243(2020).
31)Emami S. and Shayanfar A., Deep eutectic solvents for pharmaceutical formulation and drug delivery applications, Pharm Dev Technol, 25, 779-796(2020).
32)Fiala S., Jones S. A. and Brown M. B., A fundamental investigation into the effects of eutectic formation on transmembrane transport, Int J Pharm, 393, 68-73(2010).
33)Stott P. W., Williams A. C. and Barry B. W., Transdermal delivery from eutectic systems: enhanced permeation of a model drug, ibuprofen, J Control Release, 50, 297-308(1998).
34)Nyqvist-Mayer A. A., Brodin A. F. and Frank S. G., Drug release studies on an oil-water emulsion based on a eutectic mixture of lidocaine and prilocaine as the dispersed phase, J Pharm Sci, 75, 365-373(1986).
35)Maret-Ouda J., Markar S. R. and Lagergren J., Gastroesophageal Reflux Disease: A Review, JAMA, 324, 2536-2547(2020).
36)Cohen D. L., Bermont A., Richter V. and Shirin H., Real world management of esophageal ulcers: analysis of their presentation, etiology, and outcomes, Acta Gastroenterol Belg, 84(3), 417-422(2021).
37)Clarrett D. M. and Hachem C., Gastroesophageal Reflux Disease (GERD), Mo Med, 115, 214-218(2018).

38)Langtry H. D., Grant S. M. and Goa K. L., Famotidine. An updated review of its pharmacodynamic and pharmacokinetic properties, and therapeutic use in peptic ulcer disease and other allied diseases, Drugs, 38, 551-590(1989).
39)Echizen H. and Ishizaki T., Clinical pharmacokinetics of famotidine, Clin Pharmacokinet, 21, 178-194(1991).
40)Lin J. H., Chremos A. N., Yeh K. C., Antonello J. and Hessey G. A., 2nd, Effects of age and chronic renal failure on the urinary excretion kinetics of famotidine in man, Eur J Clin Pharmacol, 34, 41-46(1988).
41)Kalluri H. and Banga A. K., Formation and closure of microchannels in skin following microporation, Pharm Res, 28, 82-94(2011).
42)Grayson S. and Elias P. M., Isolation and lipid biochemical characterization of stratum corneum membrane complexes: implications for the cutaneous permeability barrier, J Invest Dermatol, 78, 128-135(1982).
43)Sharma D. S., Wadhwa S., Gulati M., Kadukkattil Ramanunny A., Awasthi A., Singh S. K., Khursheed R., Corrie L., Chitranshi N., Gupta V. K. and Vishwas S., Recent advances in intraocular and novel drug delivery systems for the treatment of diabetic retinopathy, Expert Opin Drug Deliv, 18, 553-576(2021).
44)Trommer H. and Neubert R. H., Overcoming the stratum corneum: the modulation of skin penetration. A review, Skin Pharmacol Physiol, 19, 106-121(2006).
45)Mehra K. and Geevarghese R., Formulation and Characterization of Nanotransfersome of Famotidine in Transdermal Patch, International Journal of Pharmaceutical Sciences and Nanotechnology, 8, 2814-2822(2015).
46)Doan K., Bronaugh R. L. and Yourick J. J., In vivo and in vitro skin absorption of lipophilic compounds, dibutyl phthalate, farnesol and geraniol in the hairless guinea pig, Food Chem Toxicol, 48, 18-23(2010).
47)Ono A., Azukizawa H., Ito S., Nakamura Y., Asada H., Quan Y. S., Kamiyama F., Katayama I., Hirobe S. and Okada N., Development of novel double-decker microneedle patches for transcutaneous vaccine delivery, Int J Pharm, 532, 374-383(2017).
48)Utsumi S., Obata Y. and Takayama K., Thermal behavior and functional group interaction of lipids extracted from the stratum corneum, J Drug Deliv Sci Technol, 35, 200-206(2016).

49)Olsztynska-Janus S., Pietruszka A., Kielbowicz Z. and Czarnecki M. A., ATR-IR study of skin components: Lipids, proteins and water. Part I: Temperature effect, Spectrochim Acta A Mol Biomol Spectrosc, 188, 37-49(2018).
50)Bond J. R. and Barry B. W., Limitations of hairless mouse skin as a model for in vitro permeation studies through human skin: hydration damage, J Invest Dermatol, 90, 486-489(1988).
51)Yuan X. and Capomacchia A. C., The binary eutectic of NSAIDS and two-phase liquid system for enhanced membrane permeation, Pharm Dev Technol, 10, 1-10(2005).
52)Shi Q., Wang Y., Moinuddin S. M., Feng X. and Ahsan F., Co-amorphous Drug Delivery Systems: a Review of Physical Stability, In Vitro and In Vivo Performance, AAPS PharmSciTech, 23, 259(2022).
53)Zhuang W., Hachem K., Bokov D., Javed Ansari M. and Taghvaie Nakhjiri A., Ionic liquids in pharmaceutical industry: A systematic review on applications and future perspectives, Journal of Molecular Liquids, 349, 118145(2022).
54)Zainal-Abidin M. H., Hayyan M., Ngoh G. C., Wong W. F. and Looi C. Y., Emerging frontiers of deep eutectic solvents in drug discovery and drug delivery systems, J Control Release, 316, 168-195(2019).
55)Suresh K., Mannava M. K. C. and Nangia A., A novel curcumin–artemisinin coamorphous solid: physical properties and pharmacokinetic profile, RSC Adv., 4, 58357-58361(2014).
56)Singh S. K. and Savoy A. W., Ionic liquids synthesis and applications: An overview, J Mol Liq, 297, 112038(2020).
57)Chavan R. B., Thipparaboina R., Kumar D. and Shastri N. R., Co amorphous systems: A product development perspective, Int J Pharm, 515, 403-415(2016).
58)Smith E. L., Abbott A. P. and Ryder K. S., Deep eutectic solvents (DESs) and their applications, Chem Rev, 114, 11060-11082(2014).
59)Kelley S. P., Narita A., Holbrey J. D., Green K. D., Reichert W. M. and Rogers R. D., Understanding the Effects of Ionicity in Salts, Solvates, Co-Crystals, Ionic Co-Crystals, and Ionic Liquids, Rather than Nomenclature, Is Critical to Understanding Their Behavior, Cryst Growth Des, 13, 965-975(2013).
60)Wang J., Li M., Duan L., Lin Y., Cui X., Yang Y. and Wang C., Deep Eutectic Systems as Novel Vehicles for Assisting Drug Transdermal Delivery, Pharmaceutics, 14, 2022).

61)Phatale V., Vaiphei K. K., Jha S., Patil D., Agrawal M. and Alexander A., Overcoming skin barriers through advanced transdermal drug delivery approaches, J Control Release, 351, 361-380(2022).
62)Schoellhammer C. M., Blankschtein D. and Langer R., Skin permeabilization for transdermal drug delivery: recent advances and future prospects, Expert Opin Drug Deliv, 11, 393-407(2014).
63)Bolzinger M.-A., Briançon S., Pelletier J. and Chevalier Y., Penetration of drugs through skin, a complex rate-controlling membrane, Curr Opin Colloid Interface Sci, 17, 156-165(2012).
64)Wertz P. and Downing D., Stratum corneum: biological and biochemical considerations, Marcel Dekker, Inc., (1989).
65)Shimada Y., Goto S., Uchiro H., Hirabayashi H., Yamaguchi K., Hirota K. and Terada H., Features of heat-induced amorphous complex between indomethacin and lidocaine, Colloids Surf B Biointerfaces, 102, 590-596(2013).
66)Essa E. A., Elmarakby A. O., Donia A. M. A. and El Maghraby G. M., Controlled precipitation for enhanced dissolution rate of flurbiprofen: development of rapidly disintegrating tablets, Drug Dev Ind Pharm, 43, 1430-1439(2017).
67)Alshaikh R. A., Essa E. A. and El Maghraby G. M., Eutexia for enhanced dissolution rate and anti-inflammatory activity of nonsteroidal anti-inflammatory agents: Caffeine as a melting point modulator, Int J Pharm, 563, 395-405(2019).
68)Landau R., Achilladelis B. and Scriabine A., Pharmaceutical Innovation: Revolutionizing Human Health, Chemical Heritage Press, (1999).
69)Berton P., Di Bona K. R., Yancey D., Rizvi S. A. A., Gray M., Gurau G., Shamshina J. L., Rasco J. F. and Rogers R. D., Transdermal Bioavailability in Rats of Lidocaine in the Forms of Ionic Liquids, Salts, and Deep Eutectic, ACS Med Chem Lett, 8, 498-503(2017).
70)Umeda Y., Fukami T., Furuishi T., Suzuki T., Makimura M. and Tomono K., Molecular complex consisting of two typical external medicines: intermolecular interaction between indomethacin and lidocaine, Chem Pharm Bull (Tokyo), 55, 832-836(2007).
71)Umeda Y., Kaburagi M., Furuishi T., Fukami T., Suzuki T., Tanjou K. and Tomono K., Investigation of the Percutaneous Absorption of a Novel Molecular Complex between Indomethacin and Lidocaine, Journal of Pharmaceutical Science and Technology, Japan, 69, 384-391(2009).

72)Mann S. K., Pham T. N., McQueen L. L., Lewandowski J. R. and Brown S. P., Revealing Intermolecular Hydrogen Bonding Structure and Dynamics in a Deep Eutectic Pharmaceutical by Magic-Angle Spinning NMR Spectroscopy, Mol Pharm, 17, 622-631(2020).
73)Fiandaca M., Dalwadi G., Wigent R. and Gupta P., Ionic liquid formation with deep eutectic forces at an atypical ratio (2:1) of naproxen to lidocaine in the solid-state, thermal characterization and FTIR investigation, Int J Pharm, 575, 118946(2020).
74)Moreira D. N., Fresno N., Pérez-Fernández R., Frizzo C. P., Goya P., Marco C., Martins M. A. P. and Elguero J., Brønsted acid–base pairs of drugs as dual ionic liquids: NMR ionicity studies, Tetrahedron, 71, 676-685(2015).
75)Marei H. F., Arafa M. F., Essa E. A. and El Maghraby G. M., Lidocaine as eutectic forming drug for enhanced transdermal delivery of nonsteroidal anti-inflammatory drugs, J Drug Deliv Sci Technol, 61, 102338(2021).
76)Miwa Y., Hamamoto H. and Ishida T., Lidocaine self-sacrificially improves the skin permeation of the acidic and poorly water-soluble drug etodolac via its transformation into an ionic liquid, Eur J Pharm Biopharm, 102, 92-100(2016).
77)Furuishi T., Takahashi S., Ogawa N., Gunji M., Nagase H., Suzuki T., Endo T., Ueda H., Yonemochi E. and Tomono K., Enhanced dissolution and skin permeation profiles of epalrestat with beta-cyclodextrin derivatives using a cogrinding method, Eur J Pharm Sci, 106, 79-86(2017).
78)Furuishi T., Kunimasu K., Fukushima K., Ogino T., Okamoto K., Yonemochi E., Tomono K. and Suzuki T., Formulation design and evaluation of a transdermal drug delivery system containing a novel eptazocine salt with the Eudragit® E adhesive, Journal of Drug Delivery Science and Technology, 54, 101289(2019).
79)Yataba I., Otsuka N., Matsushita I., Kamezawa M., Yamada I., Sasaki S., Uebaba K., Matsumoto H. and Hoshino Y., Plasma pharmacokinetics and synovial concentrations of S-flurbiprofen plaster in humans, Eur J Clin Pharmacol, 72, 53-59(2016).
80)Sun W., Yu J., Lu G., Ye X. and Fu J., Clinical therapeutic effects of lidocaine combination with flurbiprofen axetil for reducing propofol-induced pain in adults: A protocol for systematic review and meta-analysis, Medicine (Baltimore), 99, e23844(2020).

81)Liu X., Ma X., Kun E., Guo X., Yu Z. and Zhang F., Influence of lidocaine forms (salt vs. freebase) on properties of drug-eudragit(R) L100-55 extrudates prepared by reactive melt extrusion, Int J Pharm, 547, 291-302(2018).
82)Wei Y., Nedley M. P., Bhaduri S. B., Bredzinski X. and Boddu S. H., Masking the bitter taste of injectable lidocaine HCl formulation for dental procedures, AAPS PharmSciTech, 16, 455-465(2015).
83)Agarwal P., Nieuwoudt M. K., Li S., Procter G., Andrews G. P., Jones D. S. and Svirskis D., Exploiting hydrogen bonding to enhance lidocaine loading and stability in a poly ethylene-co-vinyl acetate carrier matrix, Int J Pharm, 621, 121819(2022).
84)Mrestani-Klaus C., Richardt A., Wespe C., Stark A., Humpfer E. and Bordusa F., Structural studies on ionic liquid/water/peptide systems by HR-MAS NMR spectroscopy, Chemphyschem, 13, 1836-1844(2012).
85)Rencurosi A., Lay L., Russo G., Prosperi D., Poletti L. and Caneva E., HRMAS NMR analysis in neat ionic liquids: a powerful tool to investigate complex organic molecules and monitor chemical reactions, Green Chem, 9, 216-218(2007).
86)Warner L., Gjersing E., Follett S. E., Elliott K. W., Dzyuba S. V. and Varga K., The effects of high concentrations of ionic liquid on GB1 protein structure and dynamics probed by high-resolution magic-angle-spinning NMR spectroscopy, Biochem Biophys Rep, 8, 75-80(2016).
87)Bica K., Shamshina J., Hough W. L., MacFarlane D. R. and Rogers R. D., Liquid forms of pharmaceutical co-crystals: exploring the boundaries of salt formation, Chem Commun (Camb), 47, 2267-2269(2011).